NASA TM-83906

NASA

Technical Memorandum 83906

NIMBUS-6 AND -7 EARTH RADIATION BUDGET (ERB) SENSOR DETAILS AND COMPONENT TESTS

FEBRUARY 1983

National Aeronautics and
Space Administration

Goddard Space Flight Center
Greenbelt, Maryland 20771

NIMBUS-6 AND -7 EARTH RADIATION BUDGET (ERB) SENSOR DETAILS AND COMPONENT TESTS

Harold V. Soule
Research and Data Systems, Inc.
Lanham, Maryland

Prepared for

Goddard Space Flight Center

by

Research and Data Systems, Inc.
Under Contract NAS5-26123

Technical Officer

H. Lee Kyle

February 1983

GODDARD SPACE FLIGHT CENTER
Greenbelt, Maryland

The requirement for the use of the International System of Units (SI) has been waived for this document under the authority of NPD 2220.4, paragraph 5.d.

PREFACE

The purpose of this document is to help the user understand the Earth Radiation Budget (ERB) sensor characteristics, their advantages and limitations. During the past decade, fragments of the ERB sensor characteristics have been published in a number of different periodicals. This complete assembly illustrating precisely how the ERB on Nimbus-6 and -7 collected radiation data should aid the user in data analysis.

Technical support in the performance of this study was furnished informally by various ERB NET members. The following individuals contributed significantly to this study.

Lee Kyle,	NASA/GSFC, Greenbelt, MD
H. Jacobowitz,	NOAA/NESS, Washington, D.C.
J. Hickey,	Eppley Lab, Newport, RI

CONTENTS

ILLUSTRATIONS

NIMBUS-6 AND -7 EARTH RADIATION BUDGET (ERB) SENSOR DETAILS AND COMPONENT TESTS

1. INTRODUCTION

The average user of Earth Radiation Budget (ERB) data is usually unfamiliar with the operating characteristics of the sensor systems that provide the data. The dissimilarity between the thermopiles (used in the solar and fixed-earth channels), the pyroelectric detectors (used in the earth-scanning channels), and traditional detectors makes it important that a basic review of their operational characteristics be made easily available. This basic information should help the user understand the advantages and limitations of the ERB sensor system.

Since ERB sensor construction details are sometimes of interest to the user and not readily available, they are given in Appendixes A, B, C, and D.

The "Design Study (Final Report) for the Nimbus-7 ERB Experiment"[1] contains most of the pertinent details regarding the ERB design history. Its historical completeness (up to December 7, 1970) makes it unnecessary to repeat the details in this 200-page report.

2. DETECTOR SELECTION

ERB radiation measurement requirements were found to be unique. These requirements included fairly uniform sensitivity to a range of wavelengths from about 0.3 to 50.0 μm and a linear response to several orders of magnitude intensity changes. In addition, an excellent long-term (months or years) response uniformity in a space environment was needed.

Pyroelectric, thermistor bolometers and thermopiles were among the several types of detectors evaluated. Based on this analysis, the thermopile was selected for the solar and fixed earth-viewing channels 1 through 14 primarily because in addition to having the desired capabilities, it also had the required response time capability. For the scanning channels 15 through 22, because a very short dwell time was available, pyroelectric sensors were used.

3. THERMOPILES

A wire-wound thermopile consists of a coil of constantan wire that is wound around an anodized aluminum heat sink. A portion of the constantan wire is copper-plated to form the thermocouples. The thermopile signals are generated by temperature differences between thermocouple junctions in intimate contact with the primary receiver and corresponding reference junctions. The reference junctions for the Eppley-type N3 thermopiles are in contact with a reference receiver which is identical with the primary receiver, but face in the opposite direction and view a relatively constant temperature housing. Thus, they are in nearly thermal equilibrium with the ERB main frame. The time constants of the primary and reference receivers are matched so that thermopile body temperature changes will not generate false signals.

Hickey[2] indicates that in the Eppley thermopile design, the best properties of two classical techniques are combined: those of the Coblentz mass compensated thermopile and those of the heat sink thermopile. The desirable qualities of these wire-wound thermopiles are good linearity, low-temperature coefficient, and long-term stability.

As with all sensor systems when extremely high radiometric accuracy is desired, many response characteristics, which are considered trivial when run-of-the-mill accuracies are adequate, become problem areas. For instance, the output signal of a thermopile is generated by the temperature difference between thermocouple junctions in contact with a black-painted radiation receiver surface and a corresponding set of reference junctions. The radiation absorption and emission characteristics of the painted surface determine the detector response. The instrument thermal design must isolate the thermopiles from spacecraft temperature changes during data-sampling periods and between channel calibration checks. Figure 1 indicates the nature of the thermal interchange between the thermopile and its surroundings. Knowledge of the module temperatures of both the solar and earth-flux channels is needed to correct for thermopile sensitivity changes with temperature. Thermistor temperature sensors and very high accuracy platinum resistance temperature sensors were installed in the thermopile bodies and in the module bodies.

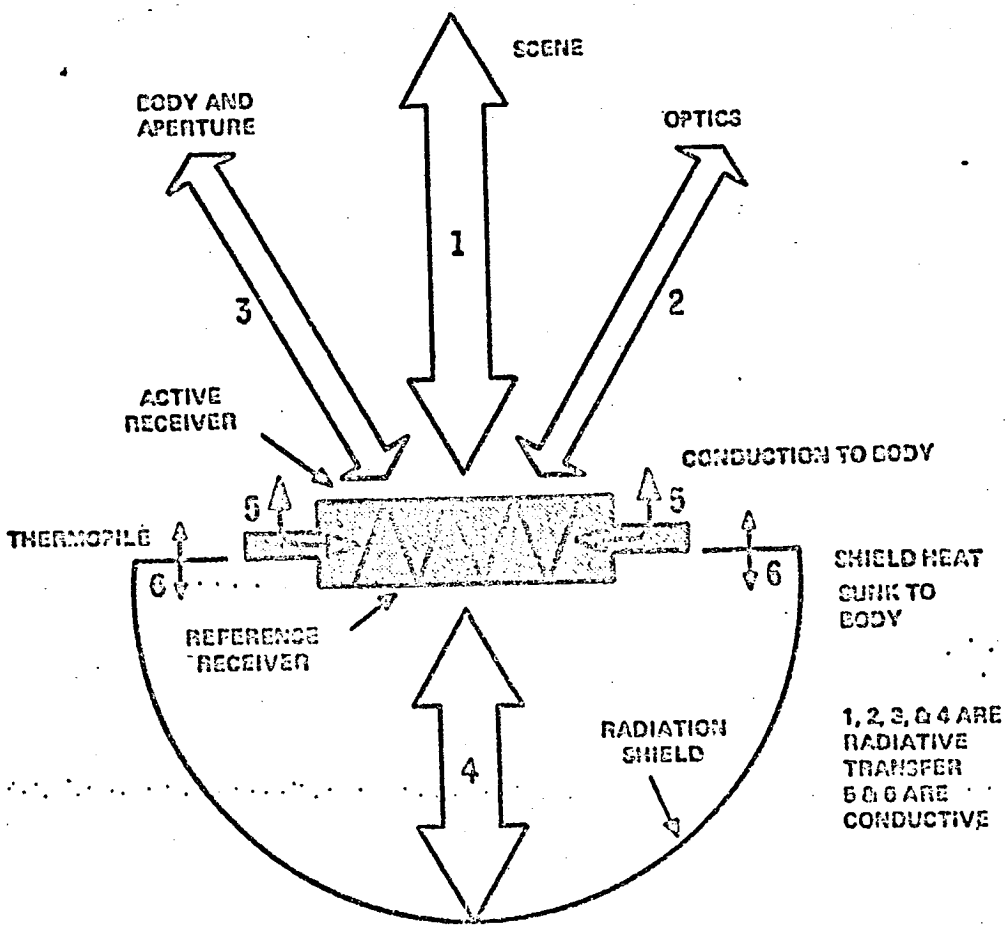

Figure 1. Radiative and Conductive Thermal Interchange for a Wire-Wound, Balanced, Heat Sink Thermopile in Vacuum When Mounted in a Typical Satellite Channel Configuration[3]

In theory and in carefully controlled laboratory tests, thermopiles have been found to have noise levels comparable to the Johnson noise of a standard resistor of the same resistance. Thus, their inherent accuracy is limited by the analog-to-digital (A/D) conversion error of one bit in 2047 and not by either the thermopile or its preamplifier.

3.1 THERMOPILE ELECTRONICS[1,2,3]

The analog chain for the thermopiles shown in Figure 2 is essentially identical for all these sensors. Since the thermopiles are dc devices, electronic chopping is used to produce an ac signal to eliminate offset effects in the amplifiers. The preamplifier converts the high-impedance, low-level signals to low-impedance signals at a higher level. To minimize noise, both the chopper and preamplifier are located near the thermopile. The post amplifier has two roles: amplification and bandpass frequency shaping. This filtering maximizes the signal-to-noise, particularly, by reducing 1/f noise. The full-wave synchronous demodulator is used to convert the ac signals back to dc. To eliminate possible switching noise transients, blanking is used. Further signal-to-noise ratio improvement is provided by the gated integrator, which integrates the signal for a fixed time. The sample-and-hold circuit stores the integrator output while the integrator is reset for the next integration period. Since the thermopile sensitivities vary approximately 20 percent from unit to unit, an initial throughput (output voltage per given input radiance) was needed to set amplifier gains so that the full-scale range was known. Absolute accuracies of a few percent and relative accuracies of 0.2 percent were required. The calibration used in the data analysis was primarily determined from extensive vacuum calibration of the whole instrument.

3.2 PROBLEM AREAS

During the design and testing of the thermopile sensor system, a considerable amount of work was required to eliminate any sensitivity of the detector to radio frequencies (RF's). This was necessary because a thermopile resembles a small multiturn loop and therefore requires adequate RF shielding and other electrical system noise pickup precautions.

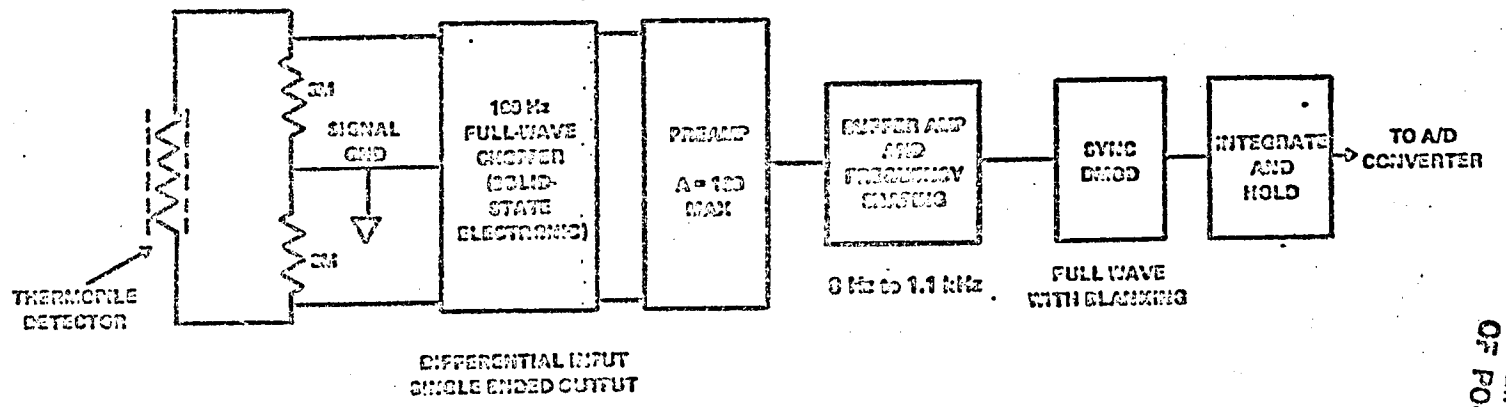

Figure 2. Analog Circuit Block for ERB Solar Channels (design developed by Gulton)[3]

4. PYROELECTRIC DETECTORS[4,5]

The pyroelectric detector was fabricated from a thin slice of a material having a permanent electrical polarization (i.e., a ferroelectric). The detector response is produced by the dependence of its degree of polarization on its temperature. However, polarization cannot be sensed on a continuous basis because a measuring circuit that is connected to the detector will allow any charge distribution to flow to the detector electrodes, neutralizing the polarization effects. Thus, the application of the pyroelectric effect relies on sensing a change in polarization. For this reason, a pyroelectric detector should be considered as strictly an ac device.

The equivalent circuit of a pyroelectric detector is a current source in parallel with its own capacitance. Therefore, a change in detector polarization will give rise to a displacement current in the detector material and a compensating current flow in the external measuring circuit.

To determine the response of the detector to incident radiation, it is necessary to measure both the effects of input radiation from a blackbody at various temperatures and the effect of sensor temperature changes. Each of these temperatures must be held constant over a range of values until a constant output sensor signal is observed. In general, the detector response is a linear function of changing input (chopped) radiation. However, the current will depend on the heat sinking of the detector element and on the response time of any coating used to enhance its radiation absorption. Figure 3 illustrates the typical response to a rectangular radiation pulse. Heat sinking causes the element temperature to approach a constant value, at which point the rate of heat loss is equal to the rate of input from the constant radiation flux. The slowing of the temperature increase corresponds to a decay (or droop) in the output current. Surface coatings produce a rounding of the pulse's leading edge.

The inherent response speed of a pyroelectric detector is due to the fact that it responds to the rate of change of temperature, rather than directly to the temperature itself. It has been noted in Reference 5 that its (3dB) frequency range is from 2 to 2000 Hz. The inherent linearity of the pyroelectric effect

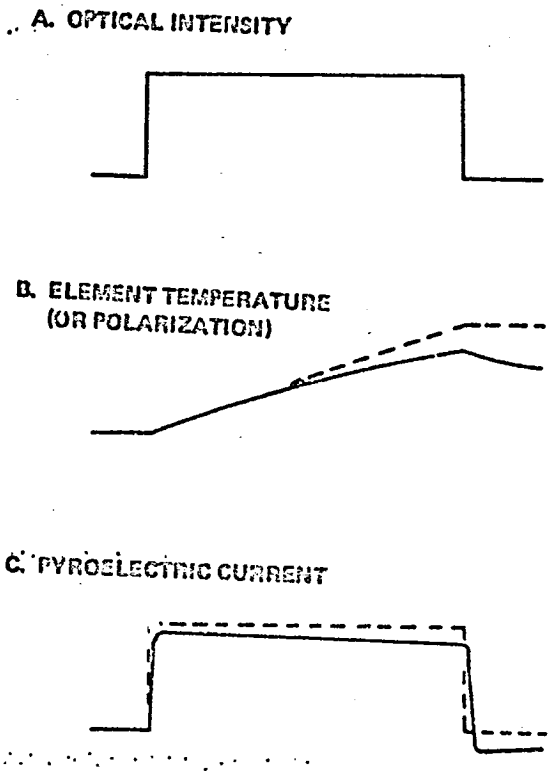

Note: Dashed lines represent the idealized case of no heat sinking (droop) or coating delay (rise time). The fast response of a pyroelectric results from the fact that the current produced is proportional to the rate of change of the detector element's average temperature.[4]

Figure 3. Response of a Pyroelectric Detector to a Rectangular Radiation Pulse

ensures that the output current is proportional to incident power even when the element heating is nonuniform. This is especially important for fast pulses, in which heating during the pulse may be concentrated near the element's surface.

4.1 PYROELECTRIC ELECTRONICS

Since the basic equivalent circuit of a pyroelectric detector is simply a current source in parallel with its own capacitance, to convert the low-level current produced by the detector to a voltage at a convenient impedance level, a high-impedance current-to-voltage converting preamplifier must be used.

It is usually very important to minimize current noise by using a high value of load resistance, or feedback resistance (typically 10^{11} ohms), and by selecting low-current leakage components. Voltage noise is also important, particularly at high frequencies or when using a large-area detector.

4.2 PROBLEM AREAS

In the ERB pyroelectric detector design, particular attention was given to the potential problems associated with the high-impedance nature of the input circuits, particularly susceptibility to electromagnetic interference and microphonics. These factors require either a hybrid detector/preamplifier design or modular construction. The latter approach allowed performance flexibility and the selection of amplifier components producing minimum noise.

An additional concern was the pyroelectric nature of the detector itself. A detector system specifically designed for low microphonics and acoustic isolation was used. The detector was firmly mounted in a relatively massive structure.

5. DETECTOR BLACK COATING CHARACTERISTICS[6]

All the ERB detector surfaces were blackened with 3M-401C10 velvet black paint. This means that the absorption/reflection characteristics of the painted sensor surface are important in determining the detector response. Both the spectral and angular response characteristics of the sensor with its painted surface should be accurately known. One of the basic reasons this

knowledge is important is that when very accurate absolute measurements of the Earth's radiation are made, fairly large temperature variations are present in the field of view (FOV). Therefore, the angular response, as well as the spectral response, is important. In addition, since the painted sensor surface radiates energy back to the Earth or space, its emission characteristics should be measured throughout the spectral regions used. Unfortunately, the spectral response out to 50 microns was not measured on either the black-painted thermopiles or the pyroelectric detectors.

Practical black coatings never attain the ideal absorptance value of unity, nor are they ever ideally free of spectral selectivity. The latter shortcoming has become more apparent during the past decade because of improvements in spectrophotometric methods. For ideal heat transfer to the underlying receiver, the thermal resistance between the front and back surfaces of the black coating should be zero, but this is also never achieved in practice. In particular, it is important to ensure during infrared measurements that the incident beam does not heat the black significantly, for it becomes difficult to distinguish between reflected and thermally remitted radiation. In any investigation regarding differences between laboratory and operational measurements, this problem should be investigated because of the considerable difference between the two data-measuring techniques.

In the mathematical long-wavelength radiometric conversion from a blackbody to an earth/atmosphere radiation spectral input, an important consideration is that the thermopiles had a very thick coating of 3M black paint, whereas the pyroelectric had such a thin 3M paint coat that the base material could be seen through the paint. This could result in quite a different long-wavelength thermopile detector response than was measured for the pyroelectric detector. Fragments of data indicate that a thick 3M coat of paint has high-infrared absorption out to long wavelengths. The lightly painted pyroelectric relative response because of increasing surface reflectivity with increasing wavelength decreased to about 40 percent of its near-infrared response[4] at 40 μm. Unfortunately, a thick-paint coat on the pyroelectric cell would have considerably degraded its performance at all wavelengths.

6. ERB SENSOR CONSTRUCTION

Since the optical characteristics of the ERB sensors is not detailed in either the Nimbus-6 or -7 Users Guide, a brief description of the construction of these sensors is necessary. A detailed description of each group of ERB sensors appears in Appendixes A, B, and C.

6.1 SOLAR CHANNELS

Figure 4 shows a cross-sectional drawing of the typical-filtered solar channel. Incoming radiation enters the sensor through a protective window. After passing through a spectral filter, it passes through a second window and strikes a 3M black-painted thermopile detector surface. The first protective window minimizes the effects of charged particles, whereas the second window reduces the effects of solar filter heating on the detector. The whole interior of the cell was painted black to reduce the effects of solar radiation reflections on the detector.

In ERB-7, a wide spectral region (0.20 to 50 μm) channel 10c replaced the very narrow bandwidth channel used in ERB-6. This channel consisting of an inverted cone within a cylinder proved very stable and radiometrically accurate.

6.2 WIDE FIELD-OF-VIEW SENSORS

Figure 5 shows the typical optical arrangement of the earth-observing wide field-of-view (WFOV) channels. The two domes provided the same charged particle and infrared attenuation filtering as was the case for the solar channels. Other WFOV channels had no hemisphere-shaped windows and sensed the entire spectral range from about 0.2 to 50.0 μm.

6.3 SCANNING CHANNELS

The ERB has four optical telescopes arranged in a fan shape which is always oriented perpendicular to the scan directions so that a wide area of Earth is swept. The telescope contains a short-wave and long-wave optical system. As shown in Figure 6, the optical hardware schematic of the narrow field-of-view (NFOV) scanning channels, the telescope focuses collected radiation alternately on one of two apertures. This is performed using a chopping wheel with

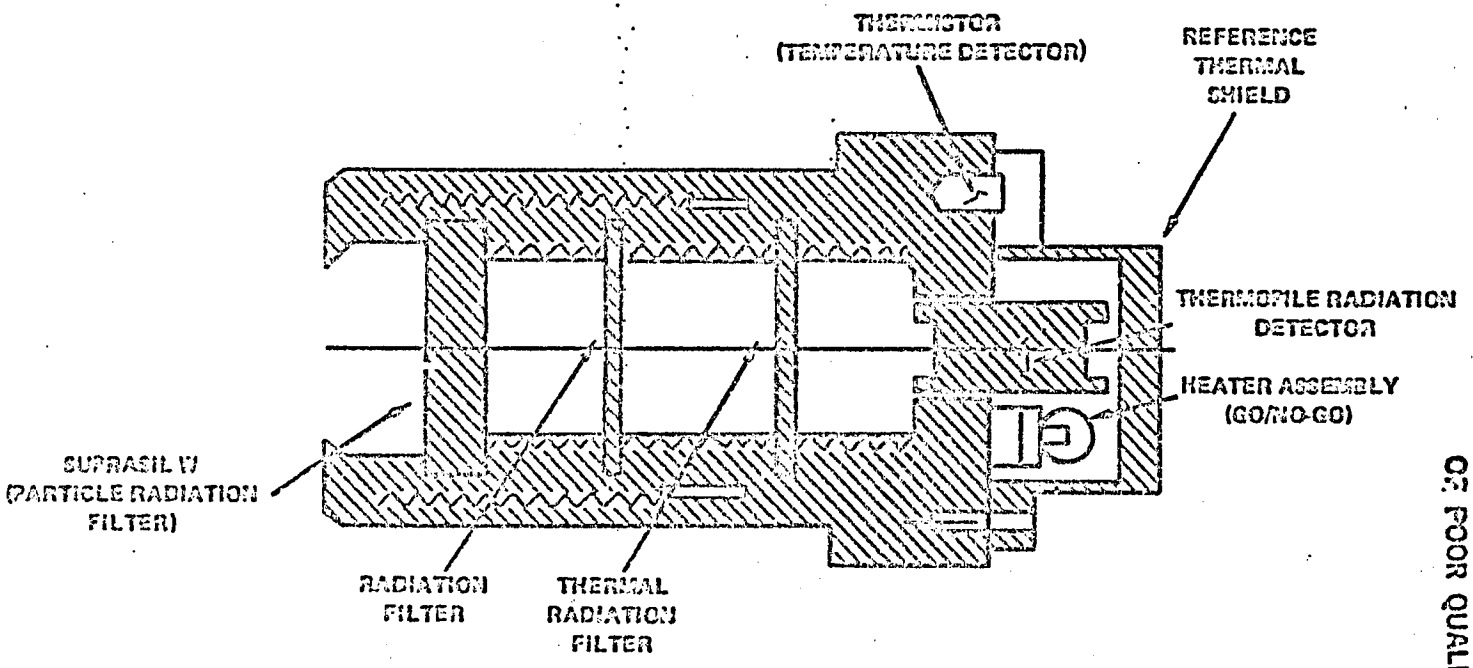

Figure 4. Typical Solar Channel Schematic (see Appendix A for details)

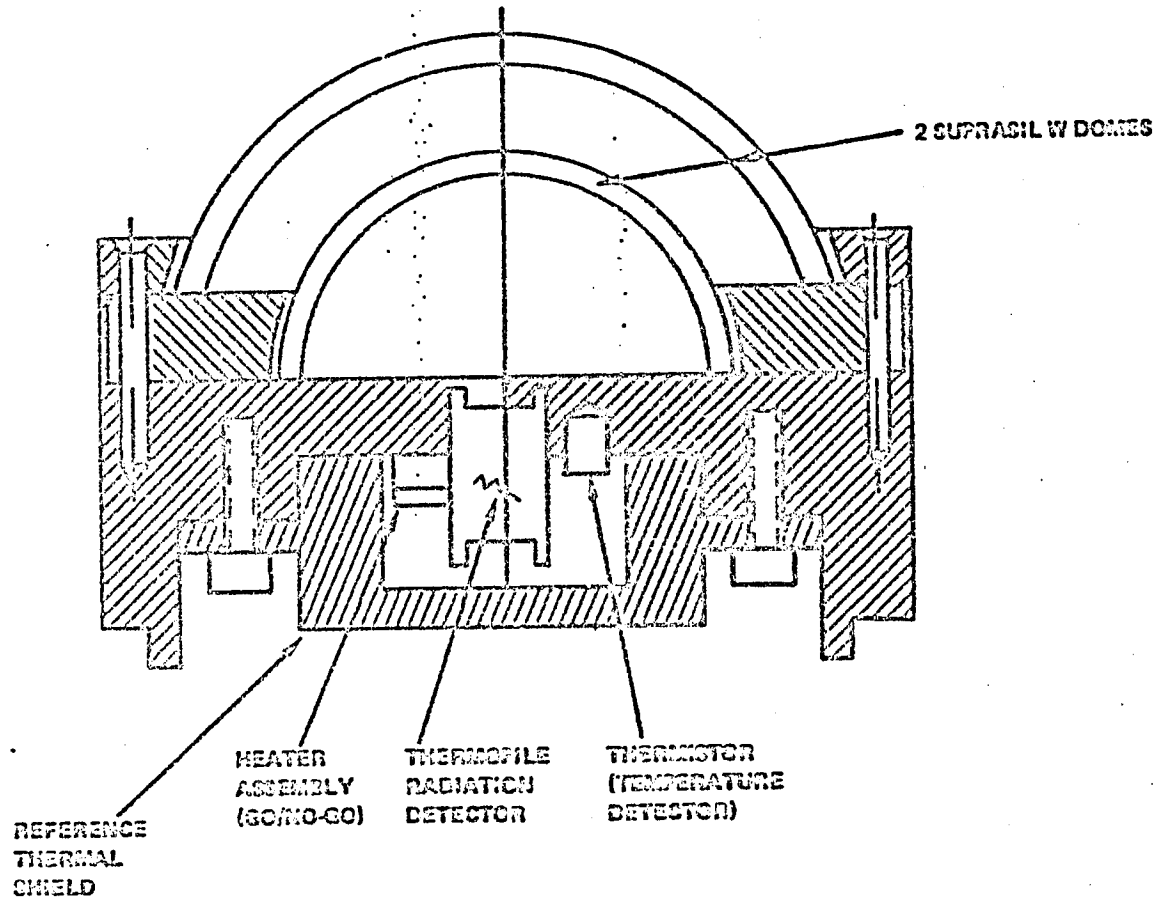

Figure 5. Typical Wide Field-of-View Earth Viewing Sensor System (see Appendix B for details)

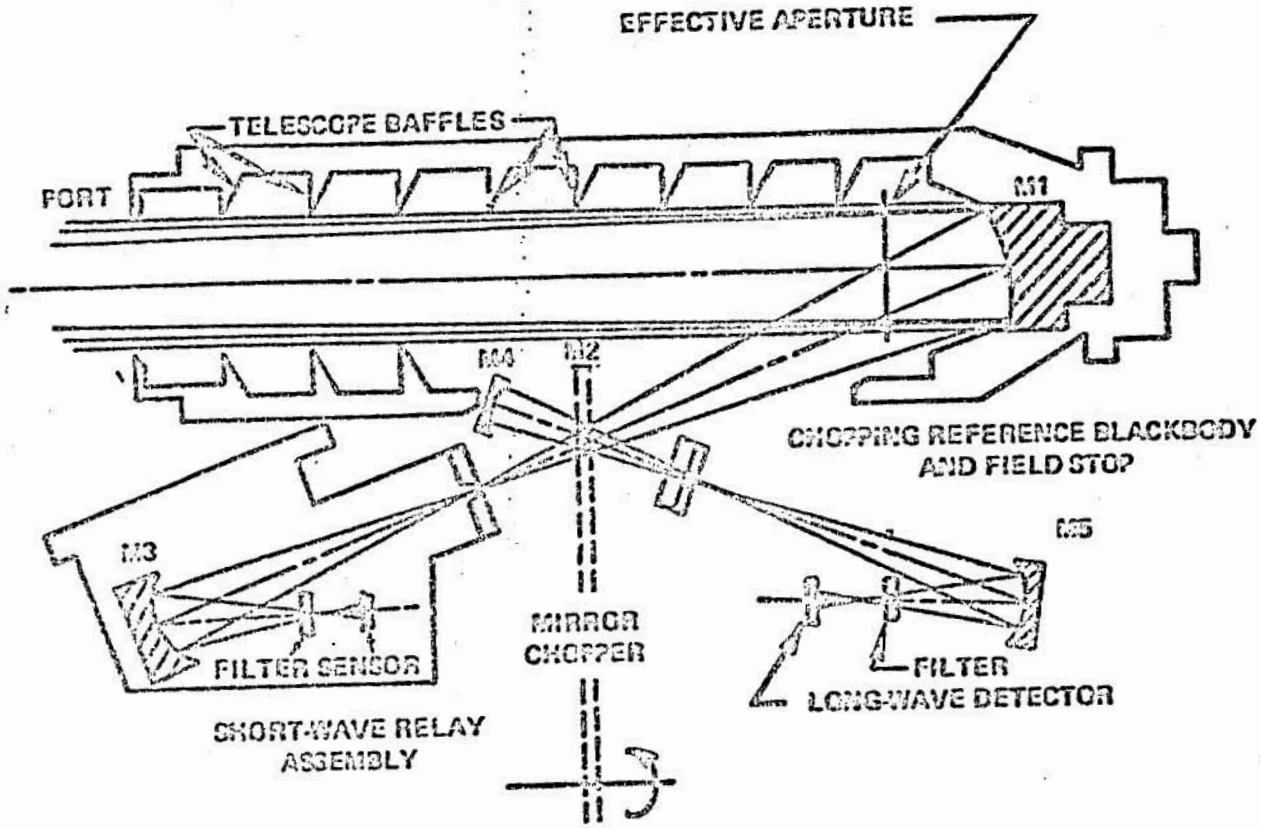

Figure 6. ERB Scanning Channel Optical Schematic (see Appendix C for details)

mirrored teeth as shown in Figure 7. When the mirrors are in the radiation beam, the radiation is reflected to the infrared optical system. The openings in the mirror teeth pass the radiation to the short-wave relay assembly. As noted in Figure 6, the short-wave relay assembly focuses reflected radiation via M3 through an appropriate filter onto the pyroelectric detector.

The long-wave portion of the scanning channels operates in a rather unique fashion. When a reflecting tooth is in the radiation beam as shown in Figures 6 and 7, the reflected radiation passing through the aperture is focused on the pyroelectric detector by the M5 mirror. It passes through a coated diamond long-wave interference filter before striking the detector.

When the openings between the mirror teeth are in the optical path, blackbody radiation from an area surrounding the aperture is reflected by M4 and focused back through the aperture slit as shown in Figure 6. This radiation is also focused through the coated diamond filter onto the detector. As a result, the pyroelectric (ac) detector senses the difference between the Earth/atmosphere or exterior blackbody radiation and the internal slit-produced blackbody radiation.

The radiation flow schematic shown in Figure 7 illustrates in detail the nature of this long-wavelength radiation measurement process. A space view and a calibrated blackbody source on the sensor system support wall are used in space to determine the long-wave detector system blackbody calibration. They produce E_{bb-1} as shown in Figure 7. After passing through the coated diamond filter, filtered radiation E_{bb-2} results. The very thin 3M black paint on the pyroelectric detector produces detector response variation with wavelength, which can also be mathematically treated as a filtering effect. This produces a theoretical radiation E_{bb-3} that heats or cools the detector. Similarly, $E_{e/a-1}$ from the Earth/atmosphere produces $E_{e/a-3}$ that alternately heats or cools the detector when the telescope views the Earth. The internal blackbody radiation E_{i-1} produced by the aperture results in the radiation E_{i-3}. The resultant counts transmitted to ground stations therefore represent the integrated spectral radiation differences between two different thermal sources.

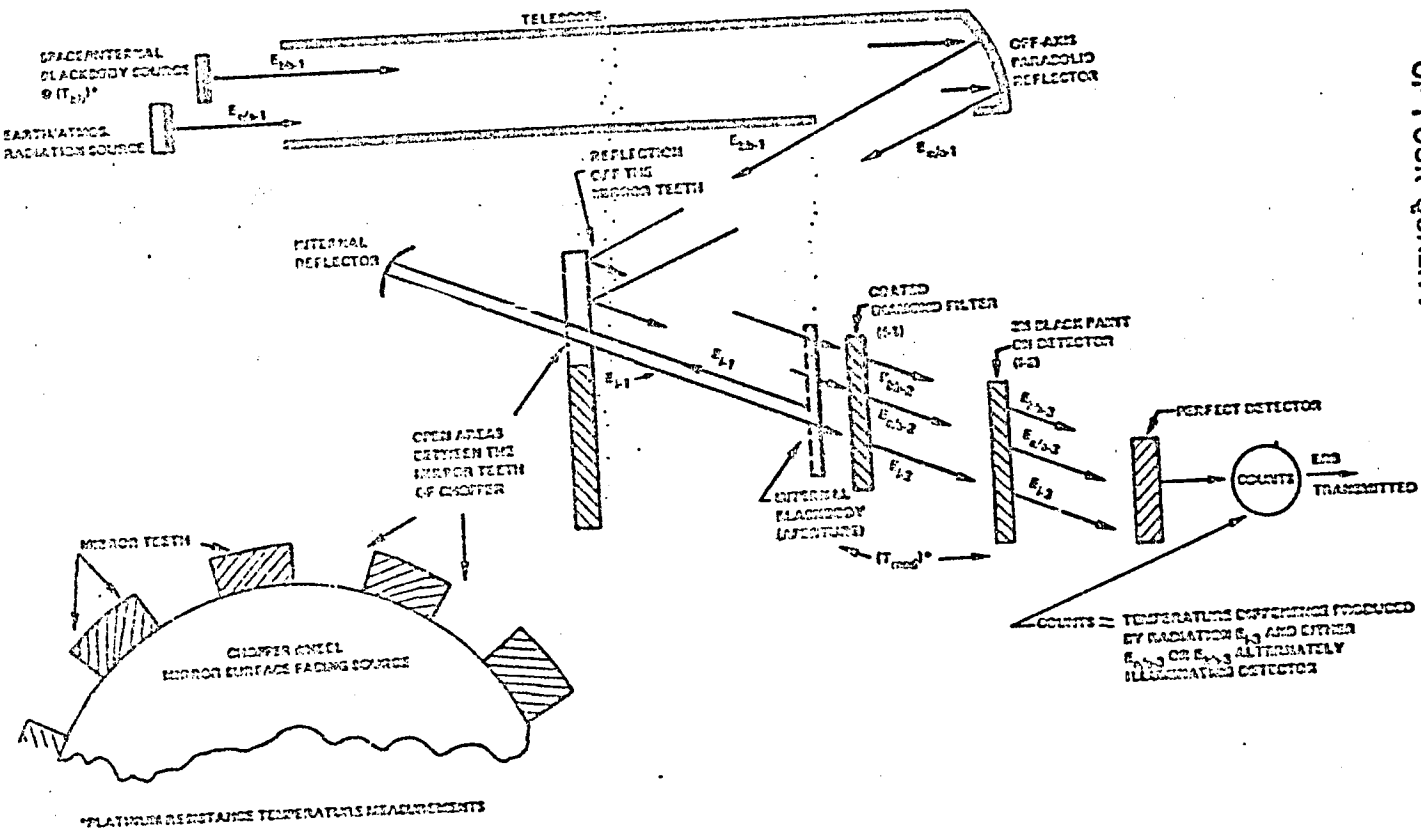

Figure 7. Scanning Channel Infrared Radiation Flow Schematic

6.4 ASSEMBLED CONFIGURATION

Figure 8 shows the location of each of the ERB sensor components. As noted, the solar channels face forward while the large FOV sensors and the scanner point down toward Earth.

7. SENSOR TESTING AND CALIBRATION[7,8]

The National Aeronautics and Space Administration (NASA) has established extensive space operational performance criteria for most of the components used in the Nimbus satellite and the ERB sensor system. Appendix E describes a few of the tests made on ERB components. Complete sensor testing and calibration were frequently combined, and complete sets of tests repeated a number of times as the problems that became apparent in the tests were corrected. Several test locations were needed because of the inherent nature of the tests and the lack of certain special facilities at each testing site. In Reference 7, the extensive details of both Eppley Lab and Gulton test requirements, preparations, procedures, and data processing are listed. The overall testing of each of the ERB components is described in Appendix D. Additional test details are given in the references. Figure 9 indicates the typical ERB-7 test plan flow diagram. Problems occurring at any of the test steps required a repeat of much of the complete cycle. Thus, 1 or 2 years were required for completing all the steps listed in Figure 9. Perhaps the most critical part of all the test procedures listed in this figure was the thermal vacuum testing of the complete satellite with all sensors in place and operating. Reference 8 indicates some of the problems that arose in this performance testing.

These tests were designed primarily to expose weak or deficient components by stressing them with temperature extremes and transients. Therefore, instrument functional checks were used to verify proper performance. Instrument function was verified either manually or visually in real time during these tests. An exception was the scan routines or patterns that required computer diagnostics. Magnetic tape records were made of each test sequence to permit post-test reconstruction of events and trends. As indicated in Reference 7, the calibration process required exercising most of the commands and functions so as to significantly reduce the amount of explicit functional testing. For time

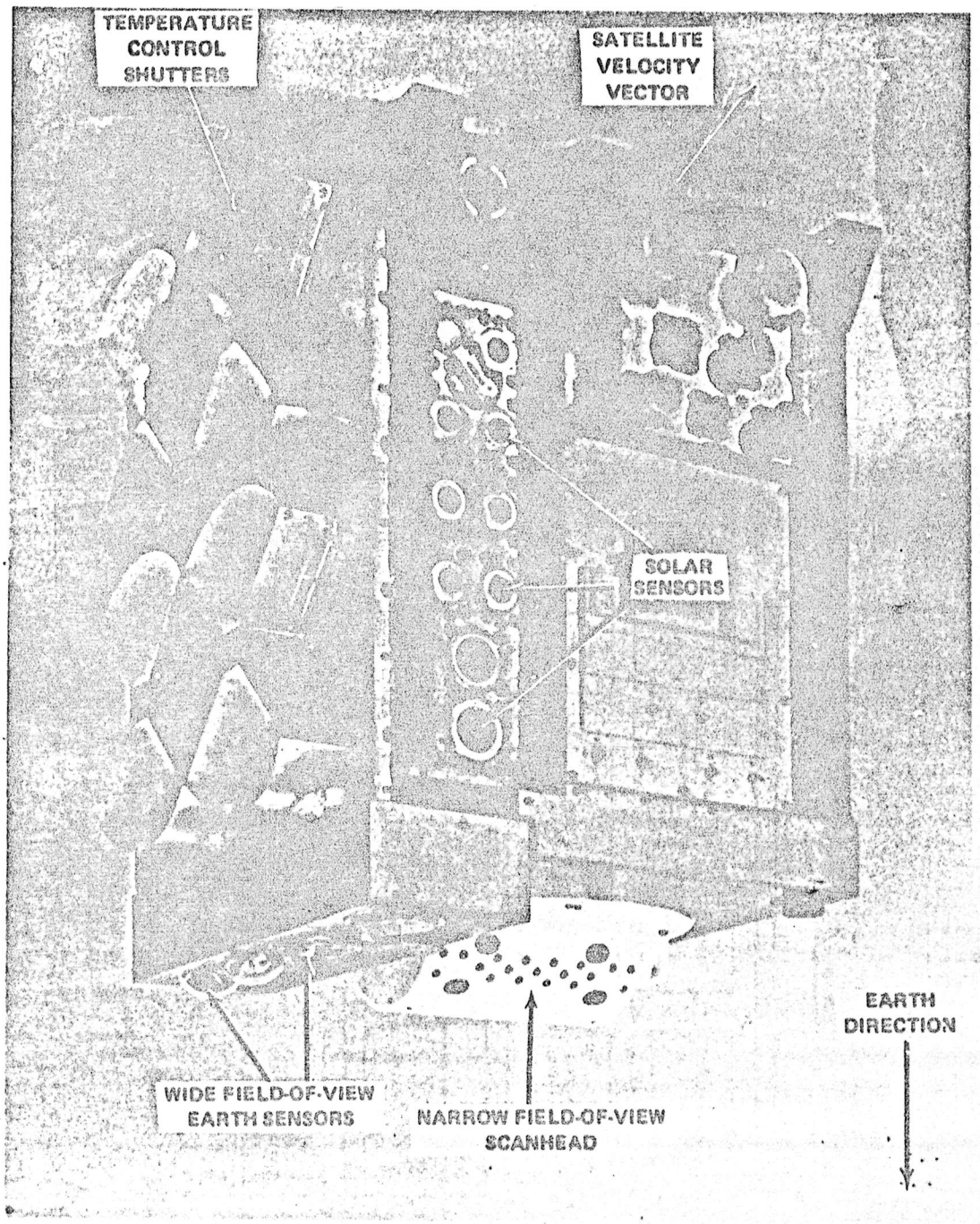

Figure 8. Complete ERB Sensor Assembly

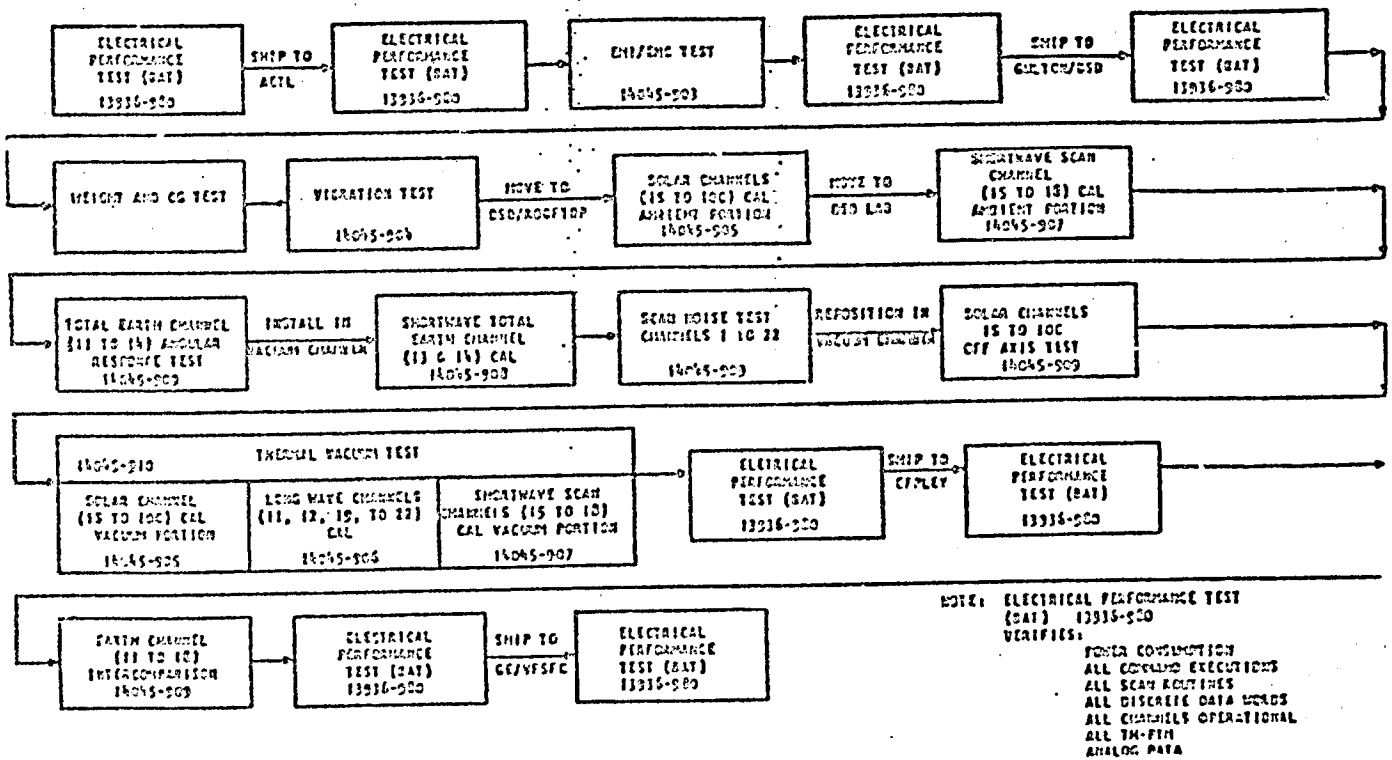

Figure 9. ERB Test and Calibration Plan Test Flow Diagram[7]

and equipment economy, vacuum calibration was usually interleaved with thermal cycling. This combination was required because temperature dependent coefficients were needed to compute orbital data. The instrument had to be accurate over a range of about 10°to 40°C. It was not physically possible to hold the sensitivities of the 22 detectors constant over this temperature range.

The desired extremely accurate ERB radiometric measurements dictated that laboratory measurements be made using standards traceable to the best international standard available at the time of the tests. Unfortunately, only recently has a "World Radiometric Reference" (WRR) become official. At the start of the ERB calibration, the most widely accepted pyrheliometer calibration was the International Pyrheliometeric Scale (IPS) of 1956. Since this scale was under revision at the time of the tests, a second pyrheliometeric reference scale was also used. This reference scale was in close agreement with the results of self-calibrating cavity radiometers.[9]

The ERB transfer standards were the Reference Sensor Model (RSM) and an Eppley Normal Incidence Pyrheliometer (NIP). The transfer standards were calibrated against both the Kendall-type PACRAD (cavity radiometer) and the Angstrom-type pyrheliometer in natural sunlight at Albuquerque, New Mexico. These transfer standards were then used in conjunction with a solar simulator and a quartz-windowed vacuum chamber to establish the final vacuum sensitivities of the ten solar channels.

Both types of transfer standards were needed because of time and spatial uniformity limitations of the solar simulator and the vacuum/air sensitivity differences of the RSM and the ERB. Many crosschecks were necessary because a direct calibration in a vacuum using a uniform solar flux was not possible. In addition to determining the basic sensitivities, it was necessary to establish a sensitivity temperature coefficient in a vacuum in the as-mounted condition in the instrument.

The traceability of the filtered solar channels shown in Figure 10 required that a set of filters matching those mounted in the ERB sensors be in the beam of the particular calibration source (usually the solar simulator) while the transmitted radiation was measured by the reference instrument. Generally this

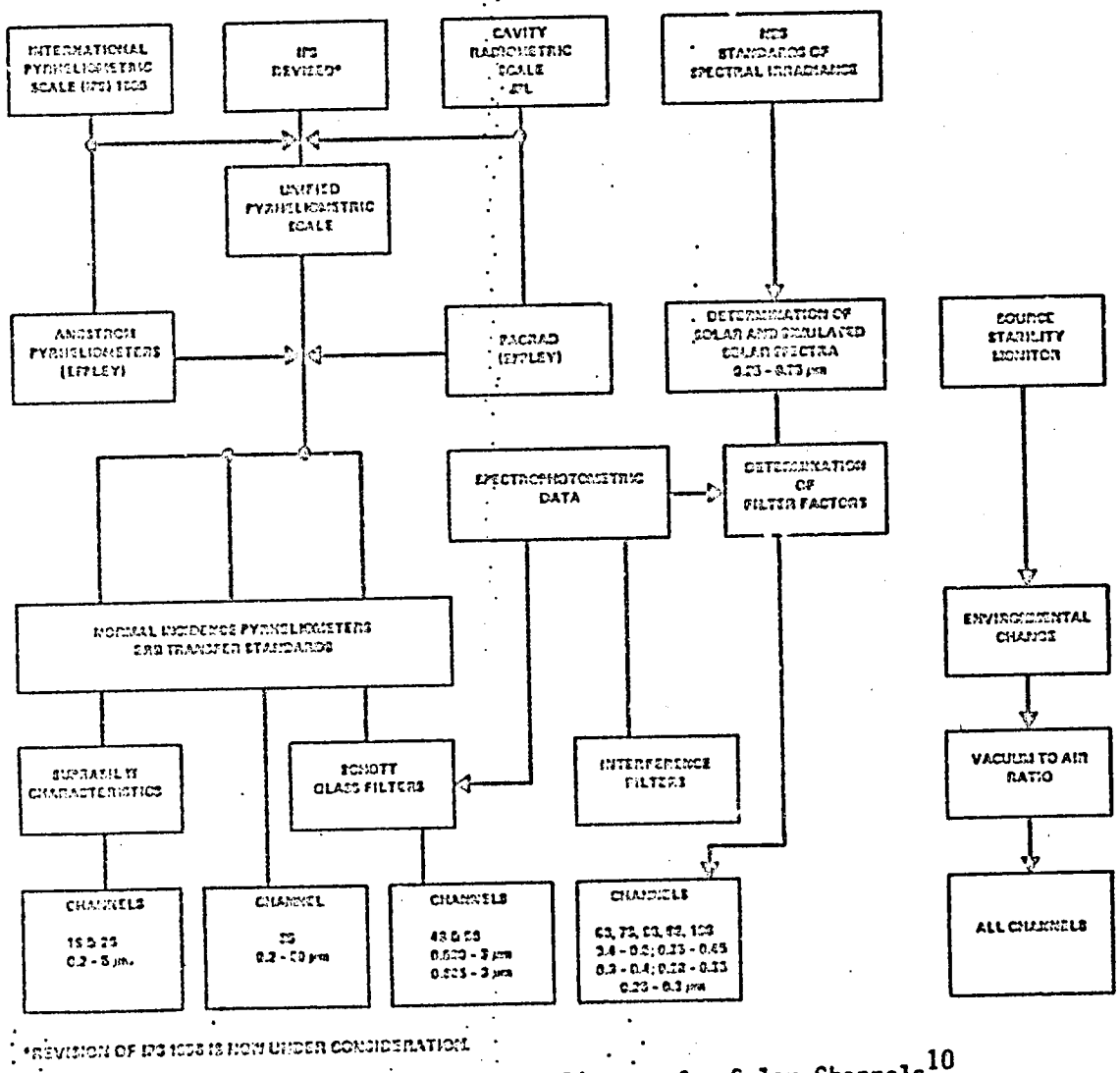

Figure 10. Traceability Diagram for Solar Channels[10]

was one of the ERB NIP's, but occasionally the cavity was used to check the results. During routine intercomparisons in the thermal vacuum testing, the ERB Reference sensor model was employed. It was also fitted with a set of matching filters. Since the spectrum of the solar simulator was different from that of extraterrestrial sunshine, a filter factor analysis had to be performed to allow for adjustment. Although this did not affect the relative work done during the various tests, it would affect the ultimate results after launch. In order to do this, the simulator spectra had to be measured using a spectroradiometer consisting of a double-prism (quartz) monochromator which viewed a standard of spectral irradiance and the simulator beam alternately. The reference lamp was traceable to the then current version of the National Bureau of Standards (NBS) scale of spectral irradiance. The transmittance curves of the filters were determined using a spectrophotometer. The mathematical convolutions were performed to determine the magnitude of the difference in filter factors for simulated and actual solar flux. Since the true extraterrestrial solar flux curve was not known, three of the most widely accepted spectra were employed in the calculations. These calculations were employed to calculate the expected transmitted energy in each band. The calculated energy was used to allow adjustment of the gain of each channel so that it would read near full scale when in orbit. The calculations were successful for all channels except channel 10s of Nimbus-6 (not a cavity) which required insertion of screen to cut down the incoming radiation.

The traceability diagram for the fixed WFOV channels shown in Figure 11 was followed in calibrating these channels. Basic blackbody calibrations were all performed in the manner indicated. The basic standard for this calibration was the International Practical Temperature Scale of 1968 as resident in the platinum resistance thermometer standard (traceable to NBS) used in the calibration of the PRT sensors in the Total Earth-flux Channel Blackbody (TECB). The problems with the calibrations using the TECB exposure technique are related to geometry and algorithm use. The geometry was imposed by the project constraints. The test environment did not allow for a true simulation of the orbital geometry and required that the radiation leaving the TECB be intercepted by ERB in such a manner that it would not interfere with adjoining instruments. The only alternative was to set the geometry so that the channels

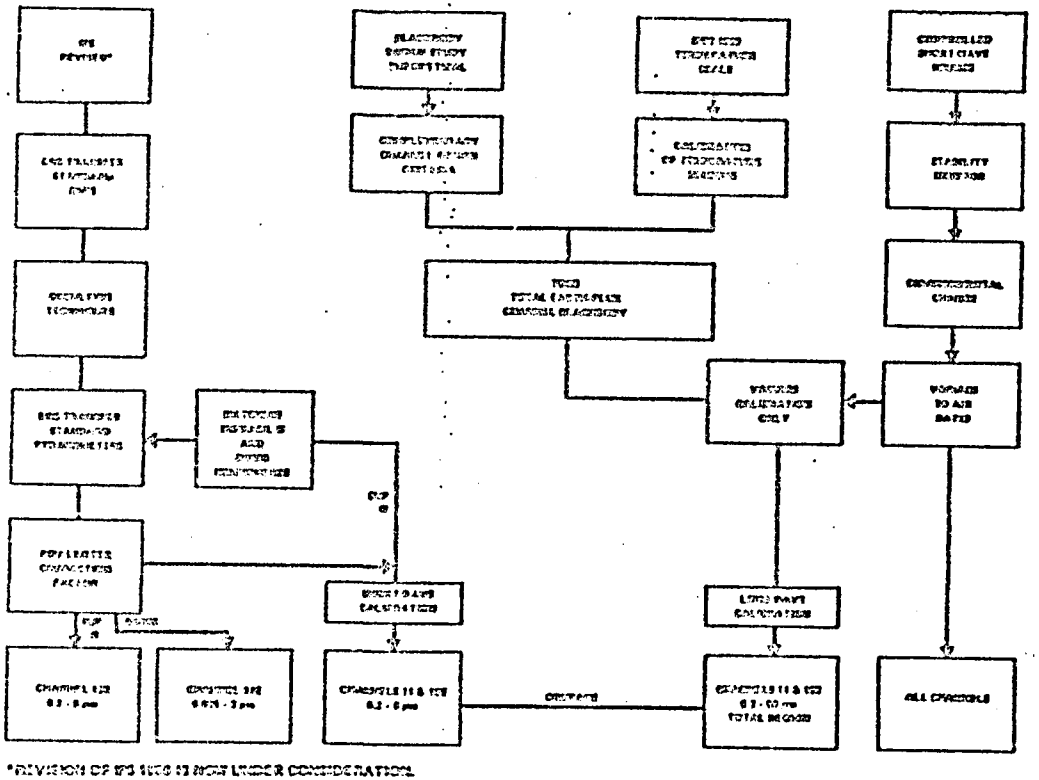

Figure 11. Traceability Diagram for Fixed Earth-Flux Channels[10]

11 and 12 were overfilled. This meant that the portion of the FOV, which would normally be filled by deep space (the annular space ring around the Earth) when in flight, was now filled by blackbody radiation from the TECB. Tests to accurately assess this effect were not performed until 1981, 3 years after the launch of Nimbus-7. The study of how to apply this new information to the flight data is still in progress.

The channels having hemispherical filters (channels 13 and 14) were essentially calibrated using techniques similar to the calibration of the solar channels. The original intent was to perform shading calibrations of the standard technique employed for pyranometers (solar radiometers with a 180° FOV), using a cavity or NIP as the reference. This proved to be impractical as did a number of other alternatives. As a result, the Nimbus-6 ERB channels 13 and 14 were calibrated in air (atmospheric pressure) on a bench in the laboratory at Gulton, using the solar simulator as the source and the NIP as the reference. For Nimbus-7, the same procedure was followed except that the tests were performed in a modified chamber under vacuum.

Figure 12 shows the traceability of the scanning channel calibrations. These channels were calibrated in terms of radiance responsivity rather than irradiance responsivity as were the solar and fixed earth-flux channels.

The short-wave scanning channels are spectrally limited to the region matching channels 1S, 2S, and 13E by matching Suprasil W windows. The calibration reference for these channels was the cavity scale through a reference normal incidence pyrheliometer. The radiance responsivity of the NIP was obtained in two ways: (1) from the calculation of the effective solid angle and subsequent application of this factor to the measured irradiance responsivity and (2) by exposure to a diffuse source of known radiance. The latter method was performed by irradiating a MgO-smoked plate with a stable beam from a solar simulator at one solar constant of total irradiance. The uniformity of the radiance field was checked by viewing the plate at a number of different angles with the instrument under test. A radiance uniformity of less than ±0.5 percent was determined in this manner. The radiance responsivity of the NIP between the two methods agreed to within ±1 percent.

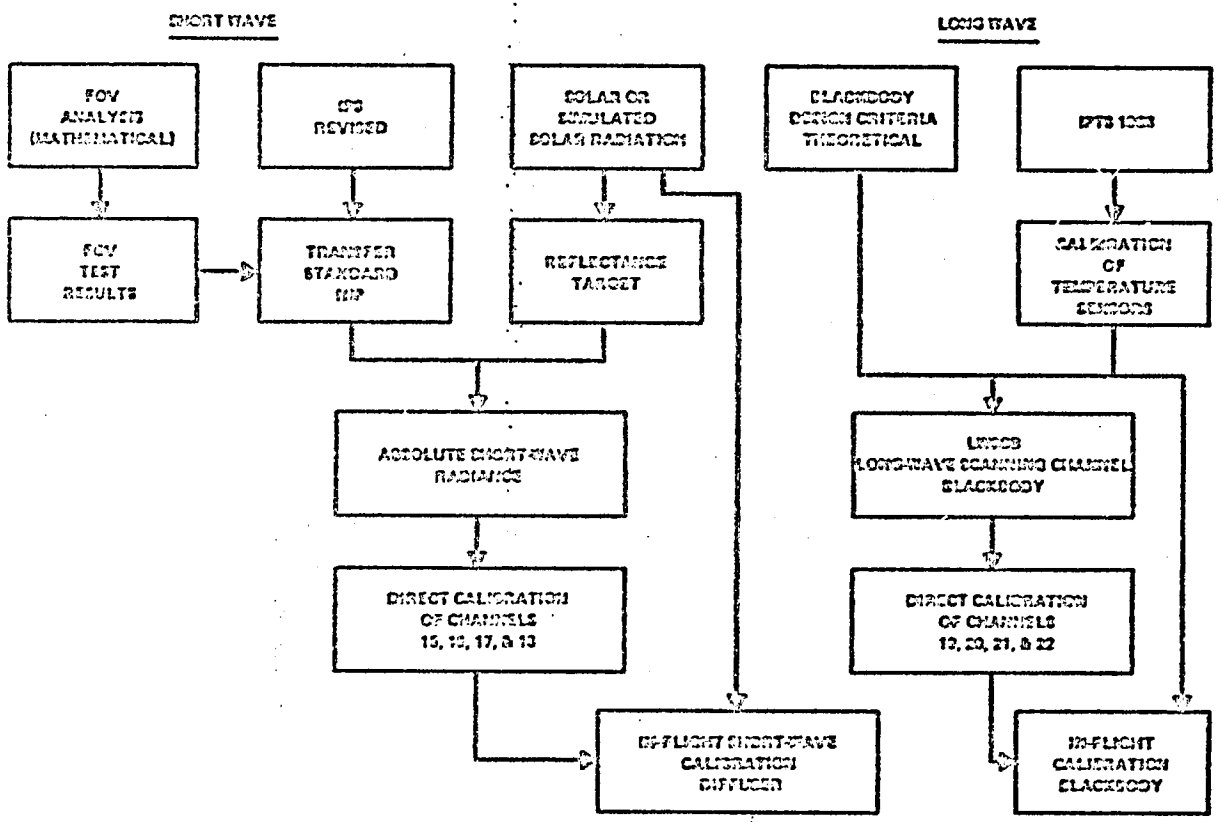

Figure 12. Traceability Diagram for Scanning Channels[10]

The short-wave scanning channels of the RSM were directly compared with a reference NIP by alternately viewing a common reflectance target that was irradiated by natural and simulated solar radiation. The reflectance target in this case was coated with barium sulfate. This procedure included monitoring the incident radiation with another calibrated NIP in such a manner that the effective reflectance of the plates for the geometrical conditions was established.

7.1 SOLAR CHANNELS 1 THROUGH 10

Solar channel calibration consisted of exposing the Normal Incident Pyrheliometer (NIP[1]) (in room air) and the Reference Sensor Model (RSM[2]) (in air or vacuum at various temperatures) sequentially to the solar simulator beam. The solar simulator was adjusted to approximately one solar constant as measured behind a quartz window identical with the vacuum chamber windows. The NIP was used to determine the solar constant.

To correct for short-term solar simulator variations, a traveling thermopile was used to instantaneously monitor solar simulator output. It was not calibrated in absolute terms. A mask was mounted in the simulator beam so that corresponding channels in the RSM and ERB used exactly the same part of the simulator beam leading to reproducible ERB/RSM ratios even in the face of spatial nonuniformities of 1 or 2 percent in the beam. Either the ERB or the RSM could be illuminated by a simple translation of the simulator.

7.2 EARTH-FLUX CHANNELS 11 THROUGH 14[8]

Calibration of the WFOV earth-flux channels fell into two categories: short-wave (channels 13 and 14) and longwave (channels 11 and 12). The calibration of channels 13 and 14 (the short-wave whole earth-flux channels) used procedures similar to those for the solar channels but required additional equipment. Physical limitations in the vacuum chamber prevented illumination of these channels from a source external to the chamber. A quartz iodine lamp was arranged to illuminate the foregoing channels in vacuum and air to establish vacuum/air response ratios. The lamp current was carefully controlled to ensure constancy during the two measurements.

Having established the vacuum/air ratios, the instrument was removed from the chamber and set up for illumination of channels 13 and 14 by the solar simulator operating at a reduced level. The simulator beam was again masked so that the beam intensity was well characterized over the small region involved. Although this approach for calibrating a wide-angle sensor differs from the reflecting hemisphere approach, it was thought to be more accurate. Available hemispheres were not suitably Lambertian or uniform to produce a better calibration.

Channels 11 and 12 (shown in detail in Appendix B) were calibrated using a highly emissive TECB, designed to fill the FOV with a uniform target temperature (no thermal gradients were present). Precision platinum resistance thermometers were used to measure the target temperatures. Target temperatures from 180° to 390° K were used in ten approximately equal radiance steps. Temperatures were controlled and monitored to 0.1° C for these calibrations. This approach established not only the sensitivity but also the linearity of the channel response to various blackbody temperatures. Calibration measurements were also performed at various instrument temperatures to establish their temperature response coefficients.

7.3 SCANNING CHANNELS 15 THROUGH 22[8]

The ERB scanning channels were the only earth-viewing channels having a flight calibration system. The long-wave infrared channels had an internal blackbody reference which could be viewed through the telescope. The short-wave channels had an aluminized flat plate which could be used to reflect solar radiance.

In the laboratory, the long-wave channels can be considered to have a dual calibration. First, they were calibrated directly in vacuum by use of a Long-Wave Scan Channel Blackbody (LWSCB). The LWSCB has four target areas that are highly emissive because they had emissive surfaces as well as geometric radiation trapping. Each target area overfilled the 0.25° by 5.14° FOV, and each area had its own platinum resistance thermometer. A target temperature 10-level calibration was performed over the range of -165° to +50°C.

The internal blackbody target was calibrated using the direct calibration of the channels as a transfer standard. In other words, by viewing first an external target of nearly the same temperature as the internal target and then viewing the internal target, the latter is calibrated directly against the external target. Since the geometry of viewing the internal target did not change, a well-defined calibration point for in-flight use was available. It is important to note that the internal target temperature readout scheme was part of this calibration. Because of the articulation properties of the scan head, the internal target was buried deep inside the instrument where it was least subject to surface degradation and was in a stable temperature environment.

The prelaunch short-wave scan channel calibration was performed by viewing an aluminized flat plate reflectance target, which was illuminated by the solar simulator. The amount of light leaving the target was determined by direct measurement using a specially calibrated NIP. Over the viewing angles used, the target was found to be very nearly Lambertian so that with knowledge of the incident radiation level, the reflected radiation could be determined. Highly reflective, freshly smoked magnesium oxide plates were used for the final calibration that verified earlier calibrations using barium sulphate plates.

This flat plate calibration target was used in space to reflect sunlight into the short-wave scan channels during calibration periods. Since the solar angle of incidence on the plate varies continuously as the spacecraft orbital position changes, the reflected radiation intensity also varies. This angle effect was determined in laboratory testing by tilting the instrument in front of the solar simulator and obtaining the sensor response ratio relative to normal incidence. Should the spacecraft yaw exceed design limits, similar yaw angle correction factors were determined over a ±20 degree range.

7.4 IN-FLIGHT CALIBRATION AND CHECKS[11,12]

In-flight checks of the degradation of the solar and earth-flux channels were accomplished by occasionally unshuttering the reference channels 1 and 11, which are duplicates of channels 2 and 12, respectively.

In addition to these optical calibration checks, the electronic linearity and gain were checked, on command, by replacing the normal varying scene signals with fixed staircase input signals. Any changes in electronic calibration were noted and corrections applied.

A go/no-go heater system provided an additional functional check for channels 1 through 14. Each of the foregoing channels has a resistor installed adjacent to the reference junction thermopile receivers. Upon actuation of the go/no-go command, a precise voltage was applied to these resistors. Since there are no shutters for channels 13 and 14, their response was contaminated by the scene. Channels 11 and 12 were influenced by the shutter temperatures that are included in the temperature telemetry points. The short-wave channels 1 through 10 were checked with the solar door shut. Although this system was designed primarily for prelaunch checkout purposes and not for calibration, its repeatability and stability were useful in long-term flight calibration confidence determinations.

Periodic in-flight checks of the short-wave scanning channel's calibration were accomplished by viewing the solar-illuminated, diffusely reflecting plate described in Section 7.3. When the scan head was commanded to "Shortwave Check," a door opened exposing the laboratory-calibrated flat plate to sunlight, which it reflected into the short-wave channels. Studies of the reflectance characteristics of this plate in space have indicated a slow steady temporal degradation even though it is securely stored behind a door between measurements.

Periodically the infrared NFOV system was calibrated by pointing the telescope at space and then at an internal blackbody having a very accurate temperature measurement system. A linear interpolation between these two blackbody radiances was used to determine the operational infrared algorithm coefficients.

In the determination of sensor drift or change in sensor response (sensitivity), the fact (indicated in Section 6.3) that the short-wavelength and long-wavelength channels operate in two entirely different modes needs emphasis. The short-wave channels operate in a conventional sensor mode, and therefore

any sensitivity change becomes apparent when correlation with other channel data is made.

In the long-wave scanning channel calibration, the counts are determined by the difference between reference radiances. Therefore, any change in sensor detectivity will not be apparent in the data using conventional analysis techniques. It is necessary to consider in detail the implications of this non-conventional data recording before it can be understood.

In the prelaunch tests, equipment limitations made it necessary to overfill the WFOV detector field of view with blackbody target radiation. Tests were made recently determining the WFOV response to the cold ring of space around the Earth, which is included in the field of view of channels 11 and 12 on both ERB 6 and 7. In these tests, a flight spare of the ERB WFOV sensors viewed a blackbody surrounded by a liquid nitrogen cooled ring. A modified algorithm allowing solutions for all calibration geometries was developed.[12]

Additional calibration checks have been performed on the ERB-7 data after the data were processed into radiance data. Among these checks are the following:

- Comparison between the WFOV and NFOV data to determine an adjustment to the original calibrations.
- Estimation of channel 13 by subtracting channel 12 night from channel 12 day when observed over a uniformly emitting surface (e.g., Tropical Pacific).[11]
- Comparison of channel 13 observations over the Sahara Desert. Channel 13 measurements were normalized for solar zenith angle and averaged over 2-week, 3-week, and monthly cycles. These values were then compared to determine the degradation of channel 13.
- Comparison of channels 11 and 12 when both are unshuttered.
- Analysis of data taken during satellite pitchup maneuvers that allow the WFOV channels to view the Sun directly.

As part of the ERB-6 reprocessing, the ERB-6 WFOV channel data are also being compared with the ERB-7 WFOV data for orbits that are approximately collocated.[13]

REFERENCES

1. National Environmental Satellite Service NOAA, "Design Study for the Nimbus F ERB Experiment," Final Report, Phase I, Contract 8-50089A, December 7, 1970.

2. Hickey, J. R., "A Satellite Experiment to Establish the Principal Extraterrestrial Solar Energetic Fluxes and Their Variance," in Extraterrestrial Solar Spectrums, edited by A. J. Drummond, et al., Inst. of Envir. Sci., 1973.

3. Hickey, J. R., et. al., "Radiation Climate Radiometer," Section 4.1.2 in Thermopile Detectors, Progress Report by Colorado State, Ball Bros., NOAA and Eppley.

4. Doyle, W. M., "User's Guide to Pyroelectric Detection," Electro-Optical Systems Design, November 1978.

5. Laser Precision Corp., "Pyroelectric Detectors for the Nimbus-F ERB Instrument TNLN108," submitted to Gulton Industries, Inc., Albuquerque, New Mexico, 1971.

6. Blevin, W. R., "Black Coatings for Thermal Radiation Detectors," Proc of Symp. on Solar Radiation, Smithsonian Inst., Radiation Biology Lab, November 13-15, 1973, p. 18.

7. Gulton/DSD, "ERB Test and Calibration Plans," Drawing No. 13936-927, in the NOOAA file at World Weather Building, August 14, 1973 (complete plans for ERB-6 tests at Gulton. Tests on the engineering reference sensor, photoflight, and flight model detailed).

8. G.E., "Nimbus F Test Report 1 and Performance Manual, Section 14 ERB," Summary of the Component Chronology including telemetry summary, electrical integration, command failures, RF noise, etc., GE Document 75SDS4223 in the NOAA file at World Weather Building, 1975.

9. Hickey, J., "Private Communication," Eppley Lab, Inc., Newport, RI., June 16, 1982.

10. Hickey, J. R., and A. R. Karoli, "Radiation Calibrations for the Earth Radiation Experiment," Appl. Opt., Vol. 13, No. 3, March 1974, pp. 523.

11. Dwivedi, P., "ERB-7 Sensitivity Study Preliminary Report, Research and Data Systems Study for NASA/GSFC," 1981.

12. Hickey, J., "Summary of Final Report on Testing of ERB Total Earth-Flux Channels and Subsequent Analysis," Eppley Laboratory Inc., Newport RI., 1982.

13. Ardanuy, P., "ERB-6/ERB-7 WFOV Comparison Study," Preliminary Report, Research and Data Systems Study for NASA/GSFC, 1981.

APPENDIX A

SOLAR CHANNEL CONSTRUCTION

APPENDIX A

SOLAR CHANNEL CONSTRUCTION

In ERB-6 and -7 there were 10 solar channels. These were independent modular elements each having only filters, apertures, and a mated amplifier. They were mounted in an array with no imaging optics. Thermopile detectors respond to temperature changes produced by solar radiation striking their surfaces. Sensor thermal emission through the aperture and to their surroundings cool them and require algorithm correction based on laboratory measurements.

1. THERMOPILE HARDWARE DETAILS[1]

The detectors for all channels discussed here were improved versions of the wire-wound type of thermopiles used in the Eppley-JPL radiometers. There were two types: N3 and K2. Type N3 is used for channels 1S through 8S and 11E through 14E. Those in the earth channels had a circular blackened area on the receiver, whereas those in the solar channels were blackened over the entire square. Channels 9S and 10S had type K2 thermopiles, which were larger but similar in construction to the N3 type. Figure A-1 is a drawing of the N3 thermopile. The identified basic parts are given in this figure.

The thermopiles were constructed to react to a conductive thermal transient in such a way that both active and reference receivers would respond simultaneously and equally to the temperature offset, thus cancelling any offset in output signal. The time constants of the actual active and reference couples were also matched by position control during the plating operation. The receivers were matched, coated, and mounted so as to ensure a time-constant balance. This requirement was extremely important because of the orbital characteristics of the experiment, since solar measurements were made during the thermal transient period due to the satellite crossing the terminator from darkness to full sunlight. It was a highly critical parameter for channels 9S and 10S, having type K2 thermopiles, because of the low-radiation input signal levels and the high sensitivity of the thermopiles. For this reason, the active and reference junction time constants of the K2 thermopiles were balanced within ±2 percent. The type N3 thermopile was balanced within ±5 percent to

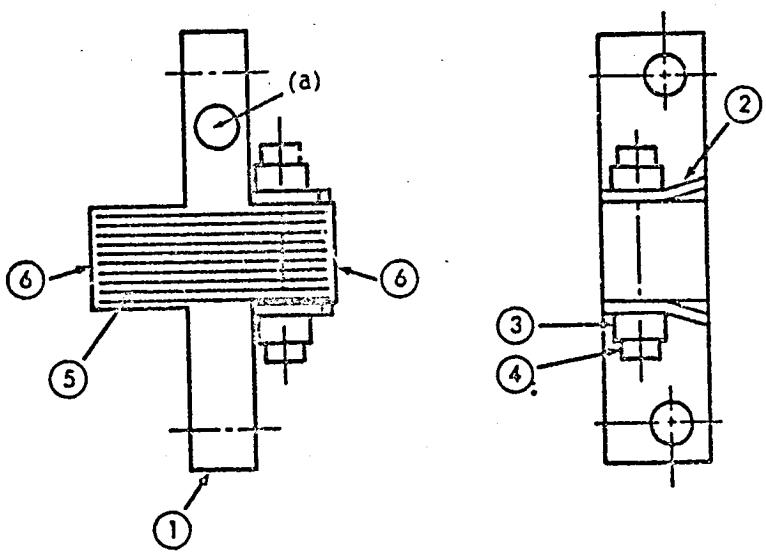

①Thermopile body (the two mounting lugs extend to either side of the main body; the top surface of the lugs is the thermal transfer control surface to the channel body)

The hole in the right lug at (a) was for mounting the monitoring thermister

②Contacts

③Insulator that electrically isolates the contact mounting screw

④Contact mounting screw

⑤Wound and plated copper-constantan thermocouple wires (the couples are made by plating copper rover a wound constantan coil in a particular manner)

⑥Active (upper) and reference (lower) receivers

Figure A-1. Schematic of the Construction of a typical Solar Sensor Thermopile[1]

meet the accuracy objectives of the other channels. The ERB-7 channels are the same as those of ERB-6, except for channel 10, which was designed as indicated in Table A-1 and described in Section 4.

All ERB-6 channels except for channels 9S and 10S had the same thermopile, type N3, whereas channels 9S and 10S had type K2. The larger size K2 thermopile was required to obtain adequate irradiance responsivity. The very narrow spectral bandwidths used for these two ERB-6 channels produced relatively small irradiance signals. The K2 thermopiles had a larger receiver area but otherwise were similar in construction to the N3 thermopiles. However, because of the larger thermisters, channel 9S and the ERB-6 10S FOV's were different from the other solar channels.

Definitions of the FOV geometry used are shown in Figure A-2. The unencumbered field is that for which the source filled the entire receiver. The central field was such that the geometrical center of the receiver was considered as a point detector, and the maximum field was that over which any part of the source could be seen by any part of the detector.

The Sun was viewed by ERB when it was within the unencumbered field for about 3 minutes over the Antarctic region. The solar channels were also monitored both before and after solar acquisition to obtain space radiation for reference use.

2. ERB SPECTRAL RESPONSE

The spectral intervals monitored by the ten ERB-6 solar channels are illustrated in Figure A-3, which are superimposed on the 1971 standard extraterrestrial NASA curve. Basically, the intervals include:

- Necessary input data for the heat budget calculations
- Bands in which deviations among various solar spectral curves exist
- Bands in which solar variability may be evident

Channels 1 and 2 were duplicates, channel 1 being the reference for channel 2 in the in-flight calibration program. Channels 4 and 5 contained broad bandpass filters that matched those of the standard Schott glasses, OG530 and

Table A-1
Characteristics of ERB-6 and -7 Solar Channels

Channel	Wavelength Limits (μm)	Filter
1	0.2 - 3.8	Suprasil W
2	0.2 - 3.8	Suprasil W
3	<0.2 to >50	None
4	0.526 - 2.8	OG530
5	0.698 - 2.8	RG695
6	0.395 - 0.508	Interference Filter
7	0.344 - 0.460	Filter
8	0.300 - 0.410	Filter
9	0.275 - 0.360	Filter
10c (ERB-7)	<0.2 to >50	None
Variation of ERB-6 from ERB-7 Solar Channels		
10s (ERB-6)	0.243 - 0.312	Interference Filter

Notes:
1. Channels 1 and 2 are redundant. Channel 1 is normally shuttered and is open periodically to adjust value of channel 2.
2. Channel 10c is a self-calibrating cavity channel added to Nimbus-7 and replacing the UV channel on Nimbus-6.
3. All are types of Eppley wire-wound thermopiles.
4. The unencumbered FOV for all channels is 10 degrees; the maximum field is 26 degrees for channels 1 through 8 and ERB-7 10c. The maximum FOV for ERB-7 channel 9 is 28 degrees and for ERB-6 channel 10 is also 28 degrees.

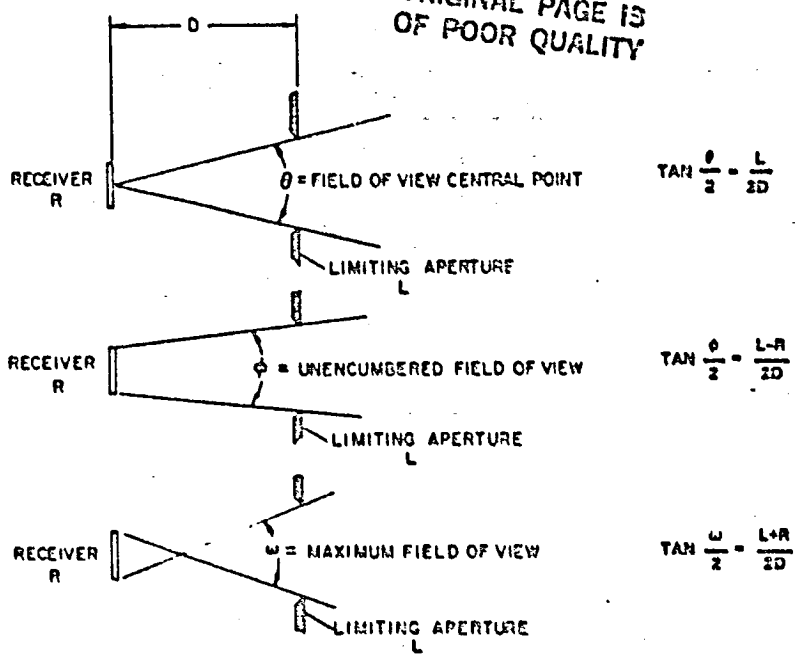

Figure A-2. Pertinent FOV Definitions for ERB Solar and Earth-Flux Channels

RG695, of the World Meteorological Organization. The filters were protected against particle radiation by 4-mm-thick windows or hemispheres of fused silica. The interference filters were deposited on Suprasil W (grade III) fused substrates to minimize degradation. Blocking outside the primary transmission bands was achieved by interference layers only. No absorbing glasses were used. The radiation in the bands λ = 0.2 - 0.53, 0.53 - 0.70, and 0.20 - 0.7 μm was obtained from the differential values of channel 4 and 5 data, together with values obtained from channel 2.

3. SOLAR CHANNEL MODULE CONSTRUCTION

The output from all the thermopiles was balanced so that the active and reference detectors produced an equal but opposite signal in response to a thermal transient. A large heat sink plus a reference detector viewing of a relatively constant temperature source permitted the active detector to accurately respond to the short-duration solar radiation.

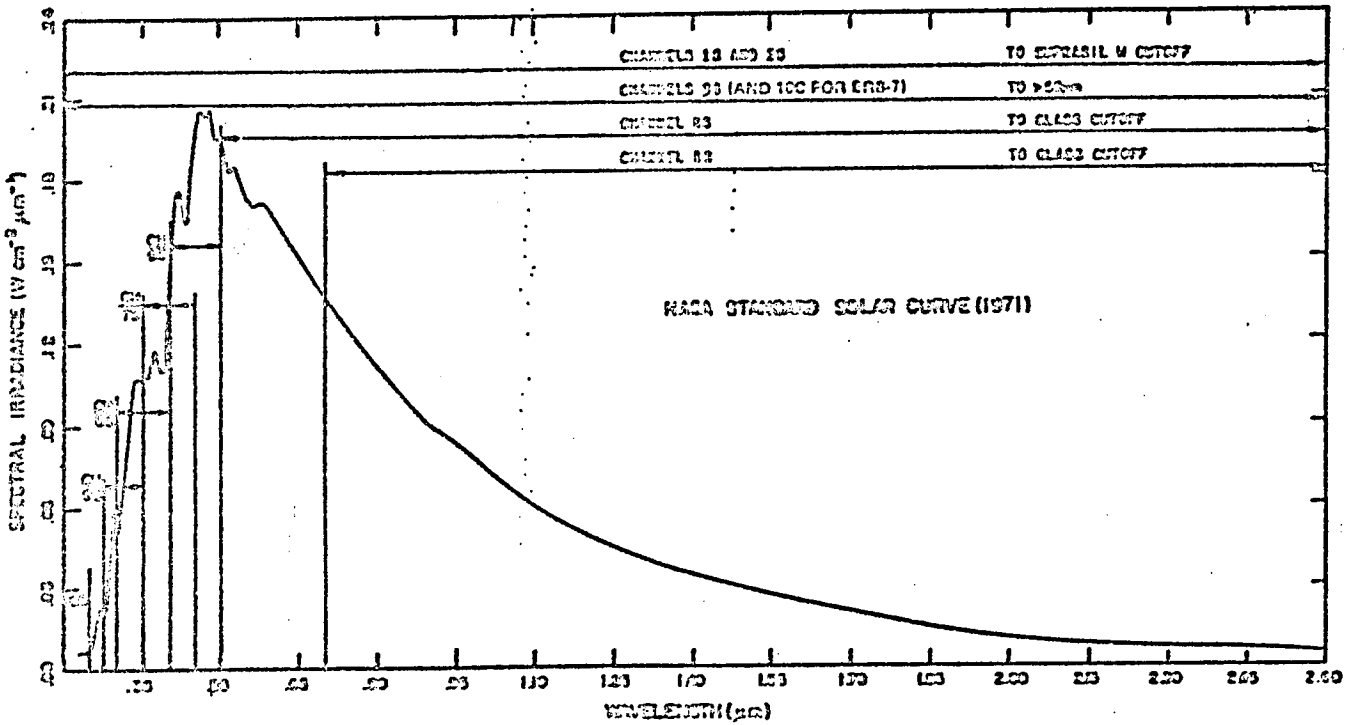

Figure A-3. Spectral Intervals Monitored by the ERB Solar Channels (with 1971 NASA Standard Extraterrestrial Solar Curve)

A cutaway drawing of channels 1 and 2 is shown in Figure A-4. The instrument body and a mounting flange had a large contact area producing good thermal conduction. At the left was the limiting aperture or aperture stop. The thermopile element was the field stop. Windows are secured by bushings that together with the wave spring washers and the retaining rings hold the two fused silica windows in place. Two thermistors for temperature monitoring were included, one in the thermopile body and the other in the module body. The flange was the mounting surface for the heat sink. The components to the left all fit within a hole drilled out of the heat sink. The blackened areas were produced by a special inorganic dye anodize applied to the aluminum pieces.

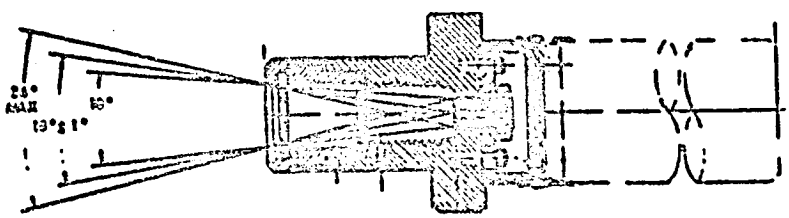

Figure A-4. Cross-Sectional View of Solar Channels 1S and 2S[1]

Proceeding from left to right in Figure A-4, the front aperture assembly is the first component. The sun-facing surface of this piece was highly polished to reduce solar radiation absorption. The second item was the forward, 2-mm-thick Suprasil W window. Behind it are its mylar gasket for protection against vibration damage and the wave spring washer that held it in place. The next large metal piece was the dual-purpose transition baffle that holds the two wave spring washers in carefully machined seats. During assembly, the rear Suprasil W window was inserted in the main baffle followed by its mylar and wave spring washers and then the transition baffle. The other components were logically mounted in reverse order with the front aperture assembly holding all components in place. A roll pin was inserted at final assembly to prevent rotation of the front aperture.

All interior surfaces of the forward areas of the channels viewed by the detector were black. In normal high-irradiance level filter radiometry, it was desirable to block all unwanted infrared radiation from reaching the detector from the baffles and other internal parts of the device. This was the reason that a quartz window was usually placed as close to the thermopile as practical. For direct beam solar measurements using filters, the largest source of unwanted infrared is usually reduced by the blocker used in conjunction with the filter.

Most materials of this type absorb a portion of the incident solar energy and reemit it as unwanted infrared. This design philosophy accounts for the two windows in channels 1S and 2S and for blockers in channels 4S through 10S.

The rear side of the mounting surface of the flange assembly was polished aluminum. The radiation shield was a copper can that was gold-plated on all exposed surfaces. The reference receiver protruded into and was completely enclosed by this gold cavity. The shield was mounted by three screws through thermally greased flanges to the channel body. Also within the radiation shield but out of direct view of the reference receiver was a "go/no-go" heater (not shown). This device was used to check thermopile response during ground testing and prelaunch procedures when light could not be used to stimulate the channels.

There were two thermistor temperature sensors in each channel, one mounted in the thermopile body and the other in the instrument body near the thermopile mounting surface. The differential measurement available from this combination permitted evaluation of the thermal sinking of the detector and interpretation of any signal offsets.

Figure A-5 shows the cutaway drawing for channel 3. It is essentially the same as those of channels 1 and 2 except that there are no fused silica windows. This channel was sensitive to all radiation from the UV to at least 50 μm in the infrared.

Figure A-6 shows the construction of channels 4S and 5S. The forward Suprasil W window was 4-mm thick. This window thickness was necessary to keep particle

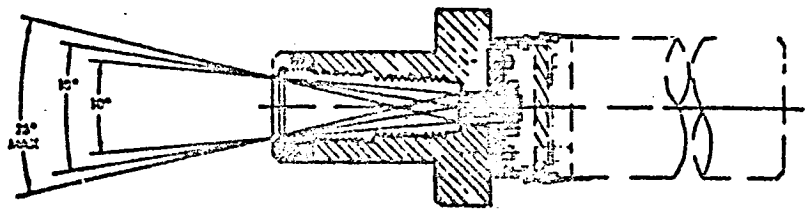

Figure A-5. Cross-Sectional View of Channel 3S[1]

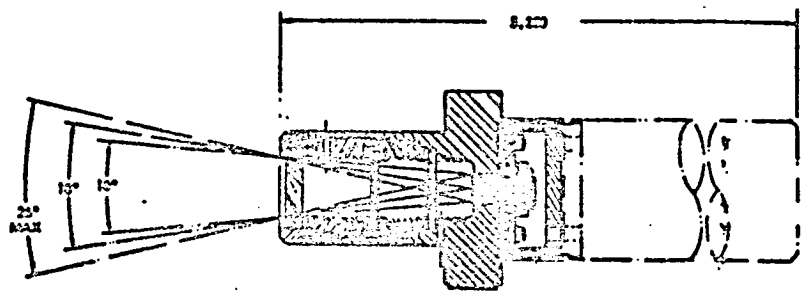

Figure A-6. Cross-Sectional View of Channels 4S and 5S[1]
(Schott glass is middle optical element)

radiation from reaching the filter window. The filter glass is the center disc of the three.

Channels 6S, 7S, and 8S were constructed the same as 4S and 5S except for the spectral band of the interference filter. Figure A-7 shows the parts for this type of channel. The interference filter (left, next to aperture) had two different-sized substrates. The 4-mm side faced the outside (toward Sun). An infrared blocker of Suprasil W was also used as previously described. The filter was placed near the front aperture rather than being used for the dual purpose of blocker and filter at the rear. Placement of the filter at the opening permitted only radiation within the passband to enter the channel. This prevented excess heating of the interior walls, and, in essence, reduced the overall heating effects within the channel. Since out-of-band rejection was primarily by reflection, the unwanted energy was removed more efficiently when the filter was as far forward in the channel as possible.

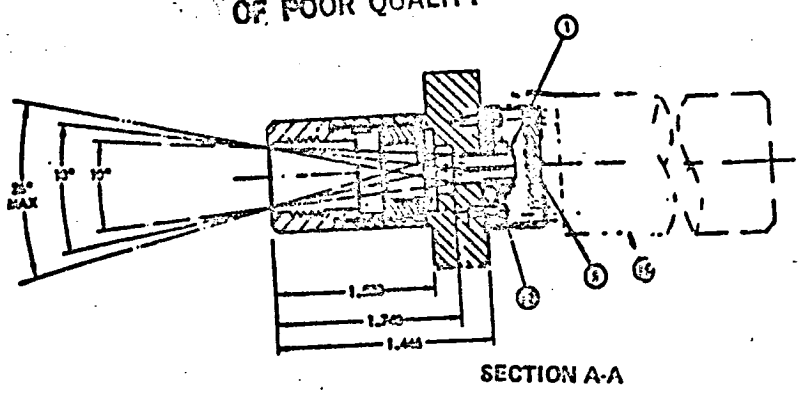

Figure A-7. Cross-Sectional View of Channels 6S, 7S, and 8S[1]
(Interference filter is front optical element)

Figure A-8 shows the components of the channels 9S and 10S. In this case, the major portion of the baffle assembly disconnects from the relatively smaller flange assembly. The active and reference receiver sections are clearly visible. In this type of channel, the infrared blocker was mounted to the flange assembly by a separate retainer ring. The filter was mounted into the baffle assembly from the rear using a separate holding assembly. The baffle and flange assemblies were then mounted together and locked with set-screws.

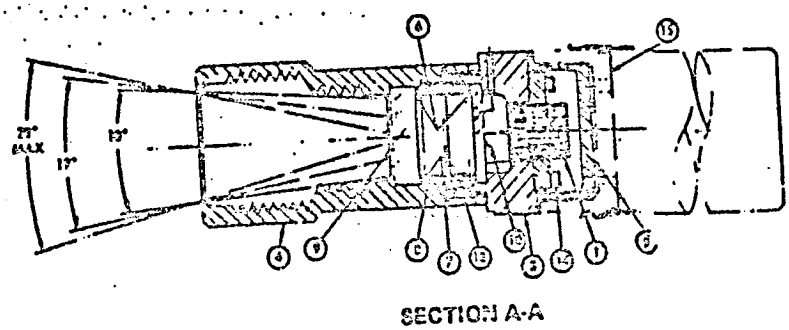

Figure A-8. Cross-Sectional View of Channels 9S and 10S[1]
(Interference filter is front optical element)

4. ERB-7 SOLAR CHANNEL (10c) CONSTRUCTION AND OPERATION[2,3]

The ERB-7 channel 10c design consisted of a thermopile with a cavity radiation receiver in front of it. This resulted in a nonsymmetric sensor with a cavity front face and a flat plate reference face. The cavity was composed of an inverted cone within a cylinder, the interior of which was coated with black paint.

Figure A-9 shows the construction of channel 10c. As noted, its interior is circular and it has an aperture at A together with baffles located along the interior of the cylinder at B. The inverted black-painted cone at C absorbs and also reflects some radiation to the surrounding wall.

The radiometer had a 10° FOV that allowed the Sun to fully irradiate the cavity for about 3 minutes during each orbit. The angular response was a cosine function. This had been proved during flight by monitoring the off-axis response relative to the on-axis solar signal. The sensor also did not experience the off-axis effects that occurred on Nimbus 6 because of an improved baffle design. Although the adherence to cosine response holds over the entire 10° field, the measurements were generally selected for an off-axis angle of less than 0.5°.

A precision electrical heater, attached to the cavity assembly, was turned on about once every 2 weeks during calibration sequences while the instrument "viewed" deep space. The sensor output was sampled once each second when the experiment was in its operational mode.

To make very high accuracy irradiance measurements, it is necessary to measure the cavity electrical heating power. In addition, the nonequivalence in sensor response to radiative and electrical heating must be measured. Thus, it was necessary to measure channel 10c cavity heater currents and voltage in addition to the sensor response. This was accomplished in the manner shown in Figure A-10.

The 10c radiometer has been very stable. The power of the cavity heater has remained stable to within 0.2 percent of the mean value. The sensitivity of

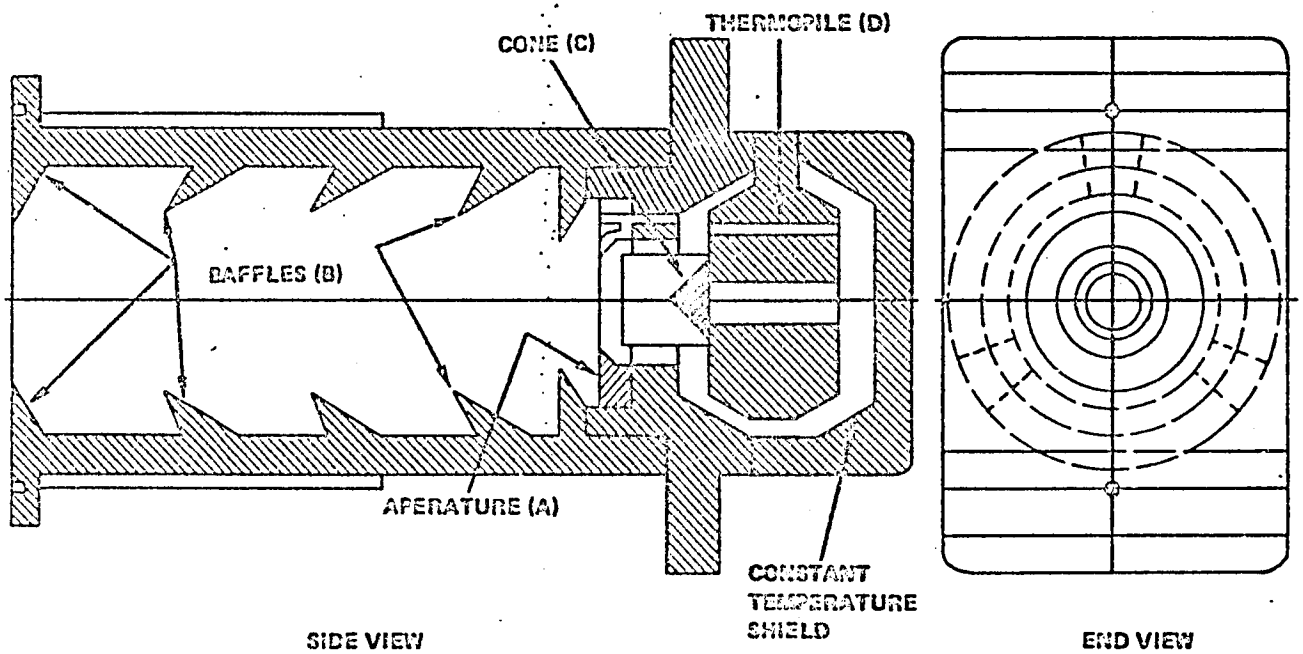

Figure A-9. Cross Sections of ERB-7 Solar Channel 10c Construction (Extracted from an Eppley Lab Blueprint)

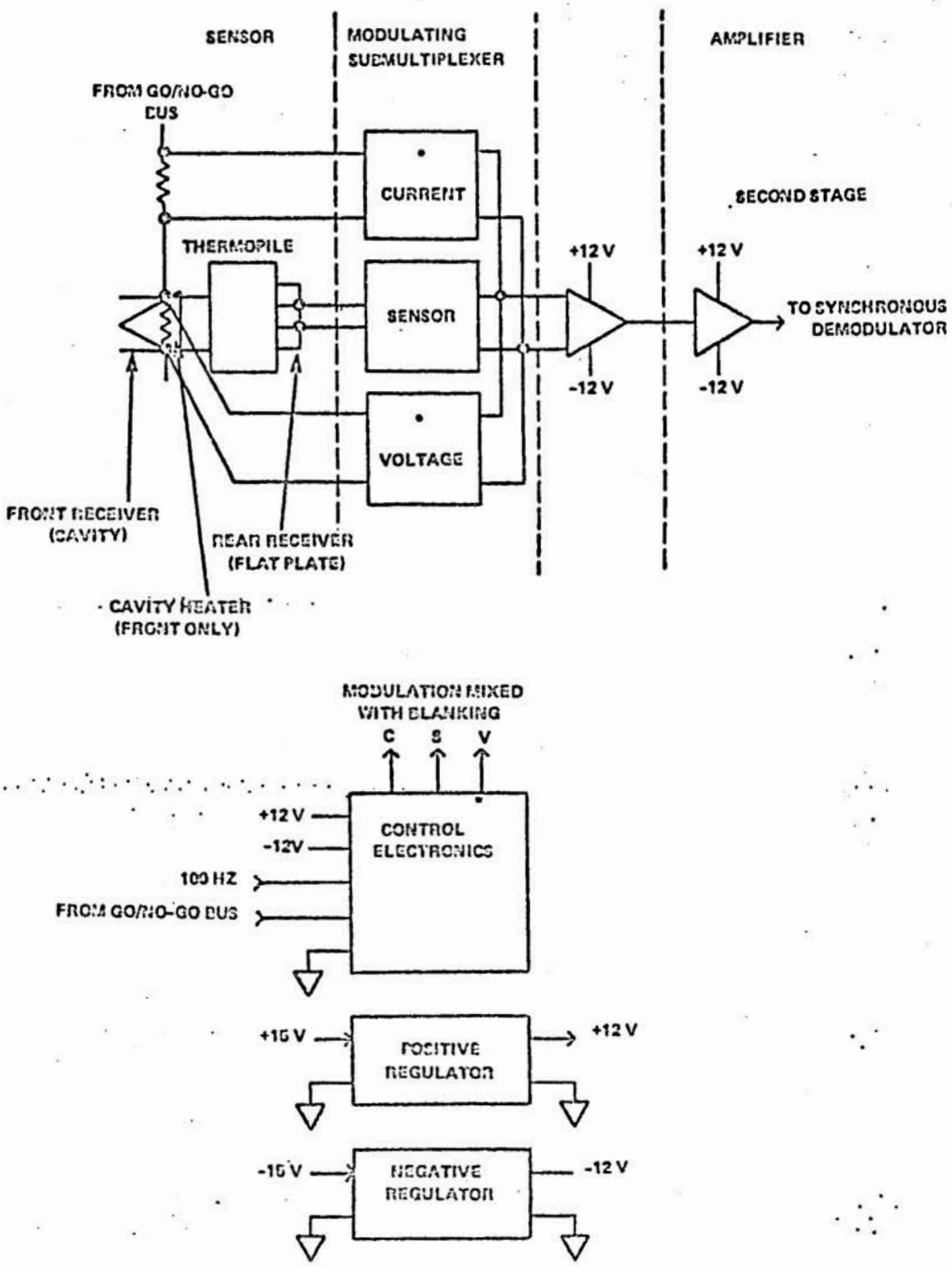

Figure A-10. Block Diagram ERB 10c Electronics[2]

the device has remained stable to 0.16 percent of the mean value after correction for temperature variations. The sensitivity determinations depend on these quantities during the in-flight calibrations. The three pertinent readings are heater current, heater voltage, and the thermopile signal. However, during solar measurement, the thermopile signal is the only sensed value.

The noise equivalent irradiance is estimated to be 0.024 Wm^{-2}, which is well below the resolution capabilities of the Nimbus ERB data system. One digital count of signal is equivalent to 0.77 Wm^{-2}. Performance is limited by the analog-to-digital converter to ±0.5 count. Thus, the uncertainty due to this limitation is about ±0.04 percent of the signal during the solar measurement. During calibration, the same limitation applies to the current and voltage readings, yielding uncertainties of 0.025 percent of their full-scale values.

5. ERB SOLAR CHANNEL ASSEMBLY AND OPERATION

The ten solar channels (1 through 10) view forward of the spacecraft in its X-Y plane. They were mounted in a solar channel assembly housing that rotated parallel to the spacecraft Z-axis. It was possible to turn the assembly by command so that its optical axes could be oriented as much as 20 degrees to either side of the spacecraft velocity vector axis permitting optimum solar data acquisition.

The ERB channel module consisted of a detector and preamplifier electronics package placed as close as possible to the detector, thus minimizing the length of electrical connections between the two units. The preamplifier was the most important component in handling small signals of the type produced by a thermopile. Short electrical lead lengths produced by close coupling reduced the possibility that thermals and other effects would produce data offsets. The method of mating the electronics can to the channel also reduced the effects of radio frequency interference (RFI) and other electromagnetic interference (EMI).

To provide space reference reading and permit electronic testing, the average counts for three major frames 13 minutes before and after solar acquisition were used. ERB-6 and -7 solar data analysis has indicated that fairly constant values exist in the data during these periods. Usable solar data were acquired

only during about a 3-minute period in each orbit when the spacecraft was over the Antarctic region.

5.1 SOLAR DOOR ASSEMBLY

The solar channels required a sun shield to shield the housing from the Sun's radiation. If a shield were not used, the housing would receive a substantial pulse of energy from the Sun causing its temperature to rise. This rise would then influence the temperature of the thermopiles that were thermally sunk in the housing. This would in turn result in an erroneous change in the thermopile's outputs. To avoid this, solar shielding was mandatory.

To protect the solar channels, the solar door assembly covered all the channels simultaneously. The device was designed principally for use in anticontamination protection and was not considered a radiometric shutter. The door was closed during all testing not involving the solar channels, all periods of transit and storage, and during prelaunch operations. The door remained closed during the launch sequence and for the first weeks in orbit. This provided solar optical protection during maximum spacecraft "outgassing." After this safety period, the door remained open most of the time.

REFERENCES

1. Hickey, J. R., "A Satellite Experiment to Establish the Principal Extraterrestrial Solar Energetic Fluxes and Their Variance," in Extraterrestrial Solar Spectrums, edited by A. J. Drummond, et al., Inst. of Envir. Sci., 1973.

2. Stowe, L., et al., "Radiometric Performance of the Nimbus-7 ERB Experiment," Tech. Improvement Workshop, Univ. of Maryland, 1979.

3. Hickey, J. R., et al., "Initial Solar Irradiance Determination from Nimbus-7 Cavity Radiometer Measurements," Amer. Assoc. for Adv. of Sci., April 18, 1980, p. 281.

APPENDIX B

FIXED EARTH-FLUX (WFOV) CHANNELS

APPENDIX B

FIXED EARTH-FLUX (WFOV) CHANNELS

1. CONSTRUCTION

There were four fixed earth-flux channels numbered 11E through 14E. Channels 11E and 12E were duplicates in the same sense as channels 1S and 2S, one being used only occasionally to check the constancy of the other. The field-of-view characteristics of all these channels were chosen to view the entire Earth's surface visible from the Nimbus orbit within their unencumbered FOV. An allowance was made for a small angular misalignment with regard to the nadir. In addition, channel 12E had a selectable smaller field, consisting of an insertable stop that permitted viewing of slightly less than the entire Earth's surface. Channels 11E and 12E were total radiation channels, with no filters or windows, permitting the measurement of absolute irradiance over the band from $\lambda = 0.2$ to 50 μm. The basic channel subassembly is shown in Figure B-1. The earthward-facing surfaces of these channels were highly polished vacuum-deposited aluminum. The channels all used type N3 thermopiles with circular receivers. They were fabricated from aluminized Kapton on which a circle of cured Chemglaze Z-306 paint had been applied and then overcoated with 3M-type 401-C10 black velvet optical paint.

Figure B-2 shows channel 13E, which was the short-wave fixed earth-flux channel. As shown in Figure B-3, it was equipped with two hemispheres of Suprasil W (grade III) fused silica. The spectral band matched those of channels 1S and 2S. The difference in radiation, measured by channel 12E with full field and 13E, was considered to be the long-wave terrestrial component (i.e., 3.8 to >50 μm).

Figure B-4 is a drawing of channel 14E, which has a broadband (RG695 glass) filter hemisphere to match the band of channel 5S. The use of RG695, as a separator of the short-wave irradiance about its cutoff wavelength of approximately 0.7 μm, has been common practice in albedo measurements. After proper correction for channel 13E and 14E measured irradiance values, the irradiance in the band $\lambda = 0.20$ to 0.7 μm was determined. Thus, the primarily scattering and absorbing regions of the short-wave reflected radiation would be independently assessed. The RG695 (partial) hemisphere of channel 14E was between two

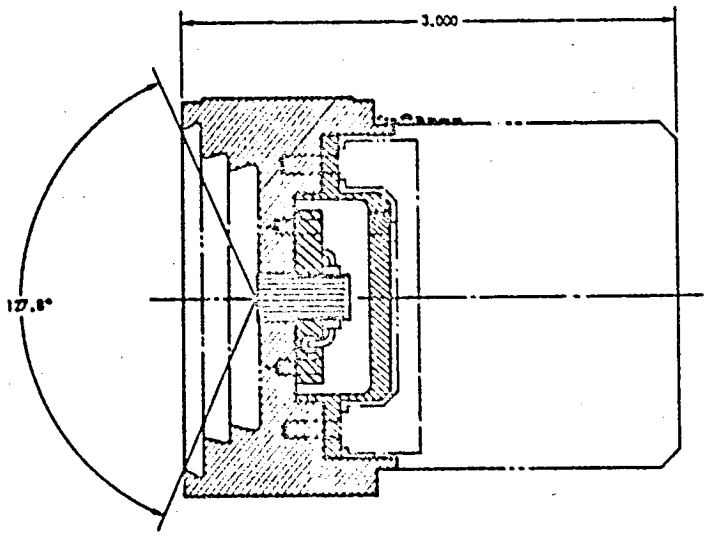

Figure B-1. Cross-Sectional View of Channels 11E and 12E (total radiation earth-flux channels)[1]

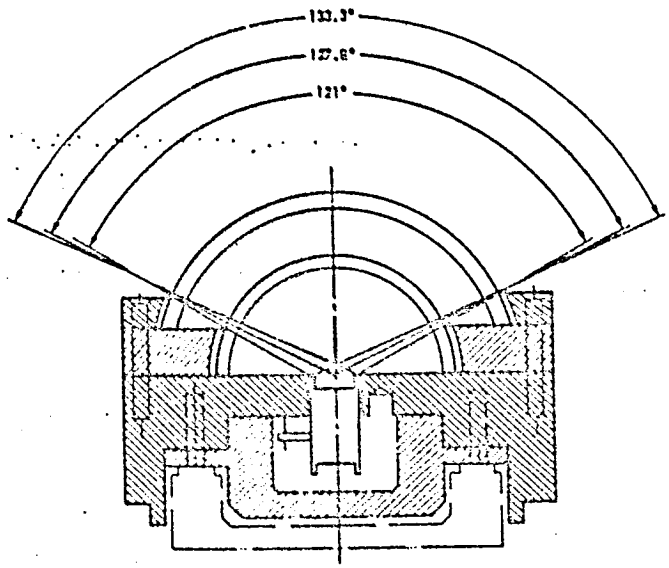

Figure B-2. Cross-Sectional View of Channel 13E (short-wavelength earth-flux channel)[1]

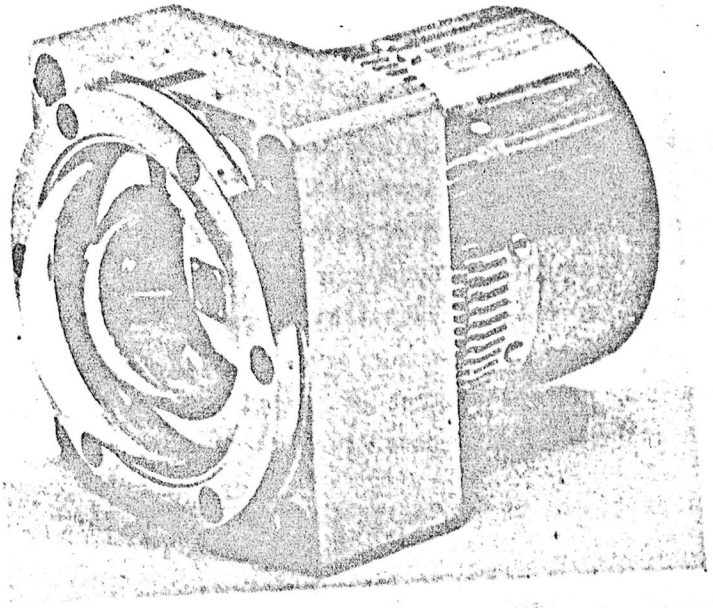

Figure B-3. Assembled Channel 13

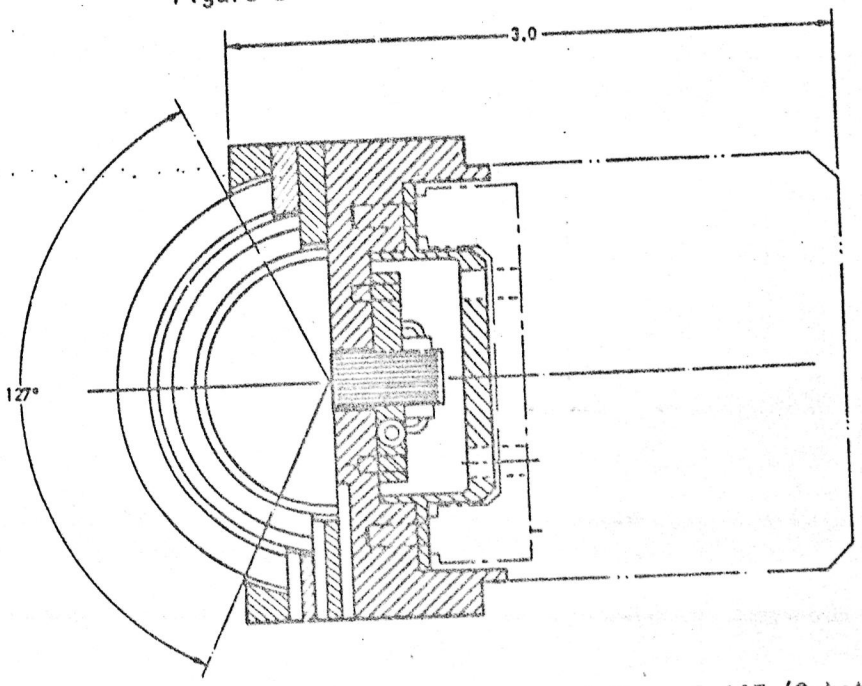

Figure B-4. Cross-Sectional View of Channel 14E (Schott RG695 glass is center hemisphere)[1]

Suprasil W fused silica hemispheres. The outer one was thick enough to attenuate particle radiation that might damage the glass. The inner dome was an infrared radiation blocking filter.

2. CHARACTERISTICS

The fixed earth-flux channels were used, in conjunction with the scanning channels, in such a manner that the integral solid angle of the measured radiance values of the scanning channels could be compared with the radiation derived from the fixed-channel data. This permitted stability and degradation checks as well as provided the opportunity to achieve the ERB scientific objective of simultaneous measurement of global and synoptic features. It also facilitated the introduction of correction factors.

Table B-1 lists pertinent characteristics of the fixed earth-flux channels.

Table B-1
Characteristics of ERB Fixed Wide-Angle FOV Channels

Channel	Wavelength Limits (μm)	Filter	Irradiance Range Anticipated (Wm^{-2})
11	<0.2 to >50	None	-200 to +600
12	<0.2 to >50	None	-200 to +600
13	0.2 to 3.8	2 Suprasil W Hemispheres	0 to 450
14	0.695 to 2.8	RG695 Hemispheres Between 2 Suprasil W Hemispheres	0 to 250

Notes:
1. Channels 11 and 12 are redundant channels. Channel 11 has black-painted baffles and is used for in-flight calibration of Channel 12. Channel 12 has polished aluminum baffles similar to those on Nimbus 6.
2. All channels have type N3 thermopile sensors.
3. All channels have an unencumbered FOV of 121 degrees and a maximum FOV of 133.3 degrees. Channel 12 has an additional FOV selection of 89.4 degrees unencumbered, 112.4 degrees maximum.
4. Output of these channels is a 3.8-second integral of the instantaneous readings.

REFERENCE

1. Hickey, J. R., "A Satellite Experiment to Establish the Principal Extraterrestrial Solar Energetic Fluxes and Their Variance," in Extraterrestrial Solar Spectrums, edited by A. J. Drummond, et al., Inst. of Envir. Sci., 1973.

APPENDIX C

SCANNING CHANNELS

APPENDIX C

SCANNING CHANNELS

1. SCANNING CHANNEL HISTORY[1]

A subsidiary of the Hughes Aircraft Company, Santa Barbara Research Center, performed the preliminary ERB scanning channel study and conceptual design work.* Scan pattern requirements and Nimbus orbit characteristic studies resulted in the unique ERB telescope design and scan patterns described in this section. This unique design developed by Gulton shared one telescope between the long- and short-wavelength sensor systems. Their use of all-reflective optics made the short-wave channel polarization insensitive.

2. PYROELECTRIC HARDWARE DETAILS[2]

The design of the ERB pyroelectric sensor system was based on the kT-4400 commercial detectors made by Laser Precision, Inc. Since space-qualified materials were used, a number of modifications were necessary. Table C-1 gives the basic advantages and disadvantages of this type of detector.

The overall design of these detectors is shown in Figure C-1. The pyroelectric crystal after being cut and polished was electroded with a vacuum-deposited nickel layer. After appropriate layer bordering, aluminum was deposited on the rear electrode. This aluminum surface determined the active area and was accurately centered relative to the crystal substrate. Lead/electrode bonding and assembly in the can support system completed the unit.

3. TELESCOPE CONSTRUCTION[1,3]

Four telescopes similar in cross section to that shown in Figure 6 were aligned so that a 12° angle separated their center lines when projected onto the horizontal plane. The instantaneous FOV of each telescope was field stop

*This design required 8 telescopes (4 long wave and 4 short wave) and crystal depolarizers.

ORIGINAL PAGE IS
OF POOR QUALITY

Table C-1
Sources of Errors in Pyrradiometric Measurements

Effects Affecting Measurements	Net and Differential Pyrradiometers: Shielded Pyrradiometers	Unshielded Pyrradiometers	Effect Affecting Accuracy of Measurement	Determination of Characteristics	References
Properties of the receiving element (black effect)	Spectral absorptivity of the black material coating the receiver		• Variation of the calibrating factor - With spectral ranges (solar and terrestrial radiations) - With the incidence of the beam (elevation and azimuth) • Change of the characteristics	• Spectrophotometric analysis of samples of absorbing coats • Goniometric analysis of the incidence effect of a light beam • Measurements of the receiver's sensitivity under variable solar incidences • Repetition of measurements at regular intervales (4 x by year)	- Reflective Products Division 3M Company Optical Product Bulletin 28, January 1967 - Eppley Laboratory Leaflet, "Parsons' Optical Black Lacquer," 1963 - Crommelynck, D., & Festraets M., "Sur la mesure de l'indicatrice de diffusion de substances tres absorbantes," I.R.M. Note technique n°6, 1971. - Crommelynck D., Festraets M., & Blon J., "Sur la technologie des mesures spectrales," I.R.M. Note technique n°3, 1971.
Properties of the shields	Characteristics of the transmissivity of cupols		• Differential variations of the calibrating factor for solar and terrestrial radiations • Effect of the incidence of the solar beam by diffusion of short-waves radiations in function of the thickness • Effect of aging and fading on the sensitivity of the receiver	• Spectrophotometric analysis: measurement of the shield's extinction • Measurement of the effect of diffuse radiation (light beam for low incidences excluding direct solar beam) • By spectral analysis, by reference to an unexposed cupol reserved for this purpose and determination of the shield's extinction	- Ambach W., Dachoner E., & Moinkes M., Uber die Eichung des Strahlungsbilanzmesser nach R. Schulze (Lupolengerat) - Arch. Met. Geoph. Biokl. series B, 13, p. 76, 1965. - Palland C. L., & Martens, "Investigations on Calibration Factors of Schulze and Funk Radiation Balance Meters and Comparison of Some Measured Results," Arch. Met. Geoph. Biokl., Series B, 18, p 93-104, 1970. - Sherwood B. Idso, "The Relative Sensitivities of Polyethylene Shielded Net Radiometers for Short and Long Wave Radiation," Rev. Sci. Inst., Vol. 41, No. 7, p. 939-945, 1970. - Collins B. G., & Kyle, "The Spectral Variation of a Polyethylene Shielded Net Radiometer," Pure and Applied Geophysics, Vol. 63, 1966.
Effect of conversion	Disturbing effect resulting from nonradiative heat exchanges between cupol and receiver - and cuple and environment (variation of the thermal resistance receiver - environment)	Disturbing effect resulting from nonradiative exchange between air and receiver (variations of the surface heat exchange coefficient)	Unchecked disturbing effects (blast of wind) that are very important for studies of the divergence of the net balance in the limit layer of the atmosphere	Study of the dynamical behavior of the instrument in terms of wind speed and air temperature in test room	- Funck L. P., "Improved Polythene Shielded Net Radiometer," J. Sci. Inst., Vol. 36, p. 267-270, June 1959. - Ross J., & Selev M., "Some Results of the Comparison of Courvoisier, Schulze and Yanishevsky Balancemeters," Geof. Pure E. Appl., Vol. 53, p. 88-100, 1962. - Suomi V. E., Franssila, M., Islitzer F., "An Improved Net Radiometer Instrument," J. Met., Vol. 11, No. 8, p. 276-282, 1954.
Effect of temperature	No linearity of the sensor in terms of temperature		Temperature coefficient	Study of thermal behavior of the instrument in air conditioned room	- Fritschen L. J., "Miniature Net Radiometer Improvements," Journal of Applied Meteorology, Vol. 4, p. 526, 1965 - Ambach et al. (voir reference susmentionee) - Dzzle P., & Guicmard R., "Mesure de l'energie solaire absorbee par le sol.," Rapport [illegible]/12 C.E.N.-CE-[illegible] de Brevet n EN7037481 du 7, September 1970 (France).
Effect of hydrometeors rain snow fog	Variations of spectral transmissivity	• Variation of spectral characteristics of absorbing coat • Heat loss by evaporation	Disturbing efforts resulting from variations of spectral characteristics and heat and no radiative exchanges	Study of the influence of rising ventilation on these effects	- Martens., Palland C. L., & Kodtsier A., "Some Experience on the Measuring of Long-Wave Radiation Fluxes," Arch. Met. Geoph. Biokl., B14, 1966. - Fritschen L. J., "Condensation on Shielded Radiometers," J. Appl Meteor., Vol. 7, p. 300-310 April 1964.
Effect of symmetry	• Non-equivalence of thermal capacities and resistances on the two surfaces of the receiver • Influence of ventilation on the two receiving surfaces		• Influence of time response of the instrument • Errors in the determination of calibrating factors for the two receivers	Testing of thermal capacities of the two surfaces of the receiver and of time constant in an air temperature conditioned room	- Schultze R., "Uber die verwendung von polyethylen fur Strahlungsmessungen," Arch. Meteor. Geoph. Biokl., B11, p 211-223, 1961. - Funk J. P., "Improved Polythene-Shielded Net Radiometer," J. Sci. Inst., Vol. 36, p. 267-270, 1959 - Suomi et al., deja mentione.
Common references including additional bibliography					- Hense W., Ein Beitrag zur Strahlungsbilanz-Messtechnick, Abh. Met. Dienstes des D.D.R. X. 76, 1965.

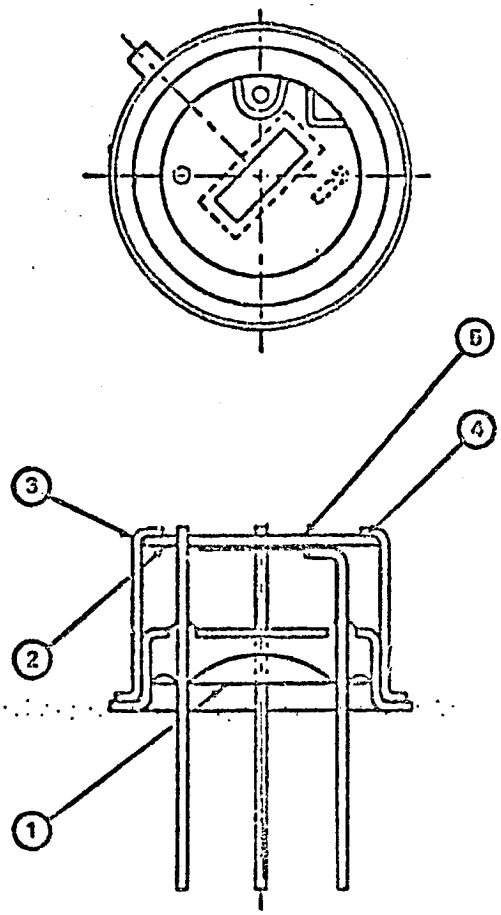

Item	Part Name
1	Header
2	Detector subassy.
3	Eyelet
4	Preform
5	Very thin layer of black paint

Figure C-1. Protype Pyroelectric Hardware Details[2]

limited to 0.25° by 5.12°. As indicated in Figure C-1, the telescopes each contained off-axis mirror objectives. A common rotating radiation chopper interrupted the focused beams just before it entered the field stops. Separation of the beam into short- and long-wavelength components was accomplished by a time-sharing beam splitter and the radiation chopper. Each telescope consisted of a field stop, spectral filter, cross-axis tilted relay mirror, aperture stop, detector, and preamplifier. With the off-axis mirror objective and cross-axis tilted relay mirror tilted equally with respect to the optical axis, the effects of reflection-produced radiation polarization were minimized. The detector was a pyroelectric element. The detected radiation was intentionally defocused to provide a uniform field response.

Different filter elements given in Table C-2 distinguised the long- and short-wave capsule characteristics. The short-wave filters consisted of a disc of Supersil-W quartz, whereas the long-wave filters used diamond substrates with dielectric coatings. The long-wave coatings were designed to block the energy in the region of the spectrum below 4.5 microns. Since the diamond substrate passed IR wavelengths out to about 50 microns, an overall 4.5- to 50-micron filter resulted.

Table C-2
Characteristics of ERB Scanning Channels

Channel	Wavelength Limits (μm)	Filter	FOV (degrees)
15-18	0.2 to 4.8	Suprasil W	0.25 x 5.12
19-22	4.5 to 50	Deposited layers on diamond substrate	0.25 x 5.12

A wide range of spectral response was obtained by coating the detectors with a black 3M paint. The detector elements consisted of pyroelectric crystals

sliced normal to their polarization axis. Electrodes were deposited on each side; then the front was sprayed with a very thin layer of 3M401 black paint.

At the detector, the beam had a cross-sectional dimension of about 0.5 mm by 3.0 mm. Areas of the detector crystal more than 0.1 mm beyond the beam envelope were not blackened. This helped reduce the off-field sensitivity.

The four telescopes had different pointing directions that were obtained by aligning the telescope at appropriate angles with respect to the scan head base plate. Fine adjustment of the FOV was obtained by a movable field stop near the primary focus of the telescope. The telescopes were of the Herschelian (offset parabola) type with specular black baffles along the barrel for stray light control. The beam bundle exited the telescope at an angle of 23° relative to the incoming beam centerline. After the beam bundle emerged from the side of the telescope, it passed through the chopping plane at an angle of about 20° from a normal through the plane. When the chopping port was blocked, this short-wave relay capsule saw the black-painted surface of the chopper blade.

The other side of the chopper blade had a gold mirror finish that efficiently reflected the long-wave energy to the long-wave relay capsule. This occurred while the short-wave capsule was blocked. The foregoing two capsules were then symmetrically disposed about the chopping plane, alternately making use of the incoming telescope beam on a 50-percent duty-cycle basis. Excellent mirror finish was obtained by depositing gold on a polished quartz blank chopper wheel.

While the long-wave capsule was not viewing the external scene, it viewed a small gold-plated mirror with an optical surface designed so that the capsule sees itself (i.e., the sensor viewed the area of the field stop portion of the relay capsule that was painted with 3M401 black and served as a blackbody reference for the long-wave channels). A platinum resistance sensor was used to determine the temperature of this reference blackbody.

The chopper had eight blades with the telescopes arranged about it so that the four telescope-produced beams were cut simultaneously. A single chopper wheel position pickup was adequate in the subsequent demodulation required for all eight signals. For the four long-wave channels, the position pickup signal was phase inverted to provide a proper output signal polarity. Chopping the optical signal resulted in a double sideband suppressed carrier system. Because of the more or less square-wave chopping, the carrier or carriers occurred at the fundamental and odd harmonics of the chopping frequency. The signal channel then had a sensitivity to noise in a band about the above carriers. A form of noise that had to be dealt with was the response of the detectors themselves to scanning channel accelerations. The final chopping frequency was set at 166-2/3 Hz after a spectral analysis of the scan head accelerations over all scan modes was made. A minimum in the acceleration response was found near the above frequency and at the first few odd harmonics.

4. DETECTOR AMPLIFIERS[1,2,3]

The pyroelectric detectors operate on the principle that a temperature change causes an electrical charge to be displaced. The resultant current was almost proportional to the temperature rate of change if the resultant current was allowed to charge the capacitance of the detector itself and the amplifier input. A triangular voltage waveform resulted from the square-wave optical chopping operation.

Design of the detector elements was a compromise between speed of response, sensitivity, and ruggedness. The mass of the crystal relative to the layer of black paint had also to be balanced so that the crystal was in fact heated by the absorbed energy. A relatively massive layer of black would result in a very small response from the crystal. By the same token, the crystal was mounted so that it is thermally isolated from a surrounding structure; otherwise, the crystal would change temperature.

The full-scale signal of the detector output was approximately 50 μV because the preamplifier was located as close as possible to the detector. The preamplifier was located on the respective delay capsules and covered by a shield.

In the scan head a few inches away from the preamplifier sensor, a gain stage amplified the signal to a level sufficient to be transmitted over the flexible cable going to the scan head. Each channel had individual signal and ground lines in this cable.

A differential line receiver-amplifier located in the central electronics produced the final gain in the channel gain string. Following this, a full-wave synchronous demodulator removed the chopping-induced carrier in the manner shown in Figure C-2. A pair of alternately operating integrators integrated the signal for 0.4 second, followed by a hold period while the outputs were digitized. Dual integrators were required because the data format did not permit insertion of the data from eight scanning channels in the 0.1 second between scenes.

In contrast to the solar and earth-flux channels, the scan channel demodulator did not use a window. The difference here was that optical chopping did not induce spikes at the crossover points as did electronic chopping.

The Phase Reference Pickup (PRP) was particularly important for proper scanning channel performance. To provide the best possible signal-to-noise performance, the PRP required calibrated adjustment. This adjustment took the form of maximizing the channel output signal for a constant scene situation. Because of the different viewing or pointing angles of the telescopes, the beam bundles did not have exactly the same centroid location relative to the chopping blade edges. The resultant compromise was an adjustment about 1 percent away from the maximum point of several channels.

The PRP signal itself was generated by a LED light source and a phototransistor pair. They were mounted so that the chopper blades passed between them and interrupted the LED beam on a 50-percent duty-cycle basis. Two independent sets of light source/detectors were available; a ground command was used to select either PRP 1 or PRP 2.

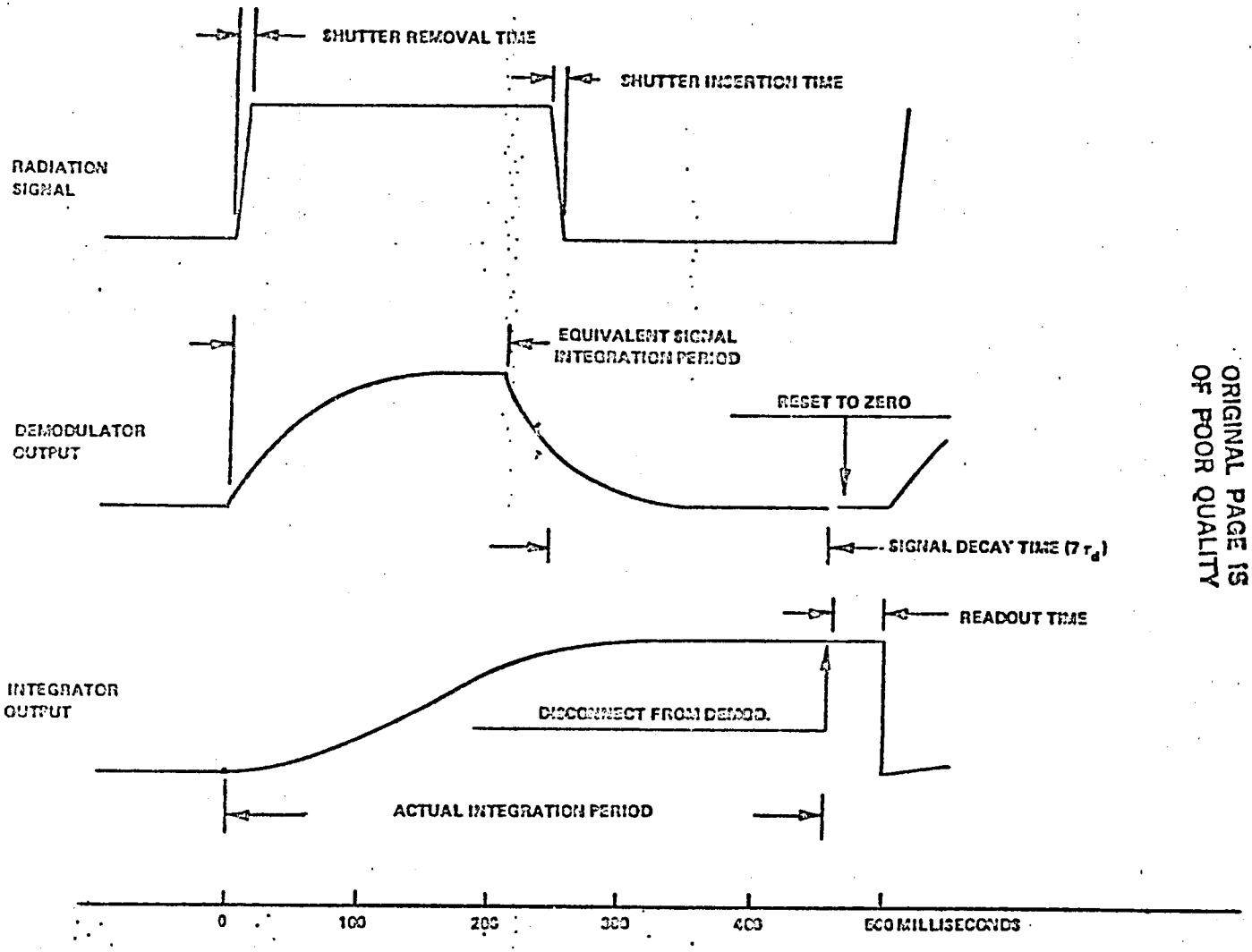

Figure C-2. ERB Scanning Channel Signals

5. SCAN ARTICULATION[2,4]

As indicated in Figure C-3, the scan head was in a gimbal mounted on the main frame of the radiometer unit. The spools of multiple lead wire between the yoke and the main frame carried the sensor power and the sensor signals. The gimbal arrangement providing the pointing direction of the scan head was specified by two angles, α and β. The angle α, in the vertical plane, was measured between the Z-axis ($\alpha = 0^\circ$) direction and the outside edge of the FOV, whereas the angle β, in the horizontal plane, was measured between the +X axis ($\beta + 0^\circ$) of the spacecraft (direction of travel) and the center of the FOV. The vertical motion was accomplished with a stepper drive motor that rotated the scan head in steps of 0.25°. The gimbal rotation was driven by a stepper motor that rotated the gimbal in steps of 0.5°. Figure C-4 shows the location of the scanner in relation to the WFOV channels.

The FOV's of the four scanning-channel telescopes were rectangular, 0.25° by 5.12°, and were arranged so that with $\alpha = 58.6^\circ$, the upper corners of the FOV's lay along the Earth's horizon. The narrow angle (0.25°) side of the FOV was in the direction of vertical (α) motion. The FOV's of the long-wavelength channels 19 through 22 were coincident, respectively, with those of the short-wavelength channels 15 through 18. Thus, an arc segment having a radius equivalent to the Earth's horizon when viewed from the spacecraft passed through the long dimension of the field. The primary scan sweep was along the 0.25° direction. By indexing the scan head 5.12° between the up and down sweeps, total coverage was obtained over the area scanned.

The scan pattern generator had four basic duties: the pattern determination, beta position initialization, and incremental alpha and beta motion logic. Each selected pattern contained a sequence of long-, short-, and long-grid motion. This sequence was repeated once for each of the four basic patterns. The fifth pattern was a compound pattern, the performance of the third followed by the fourth pattern. Long-grid motion caused the scan sensor group to sweep to the local Earth's horizon and beyond, then return in a symmetrical fashion about the space-viewing position. Short-grid motion caused the scan

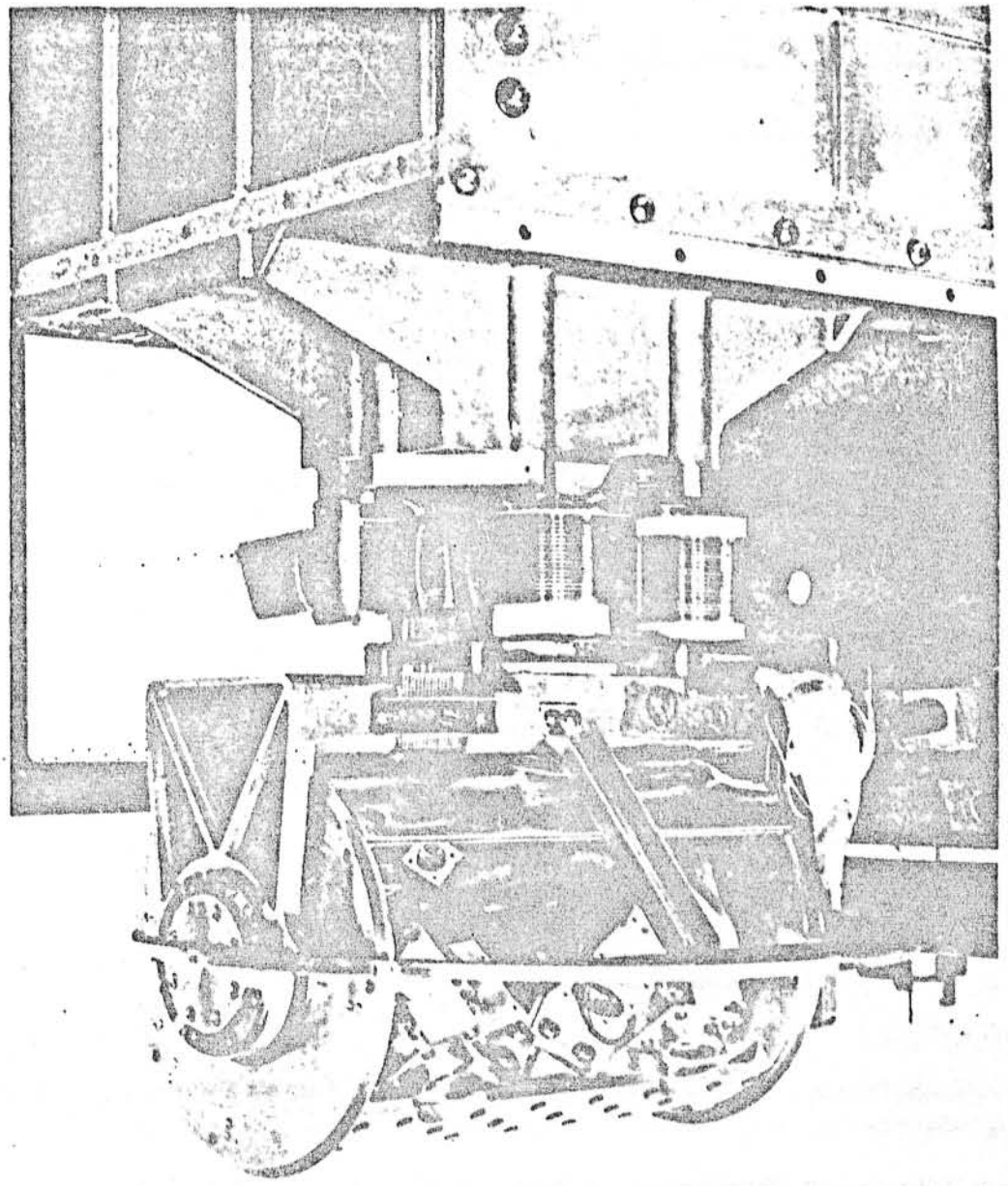

Figure C-3. Scan Hardware with Electrical Leads

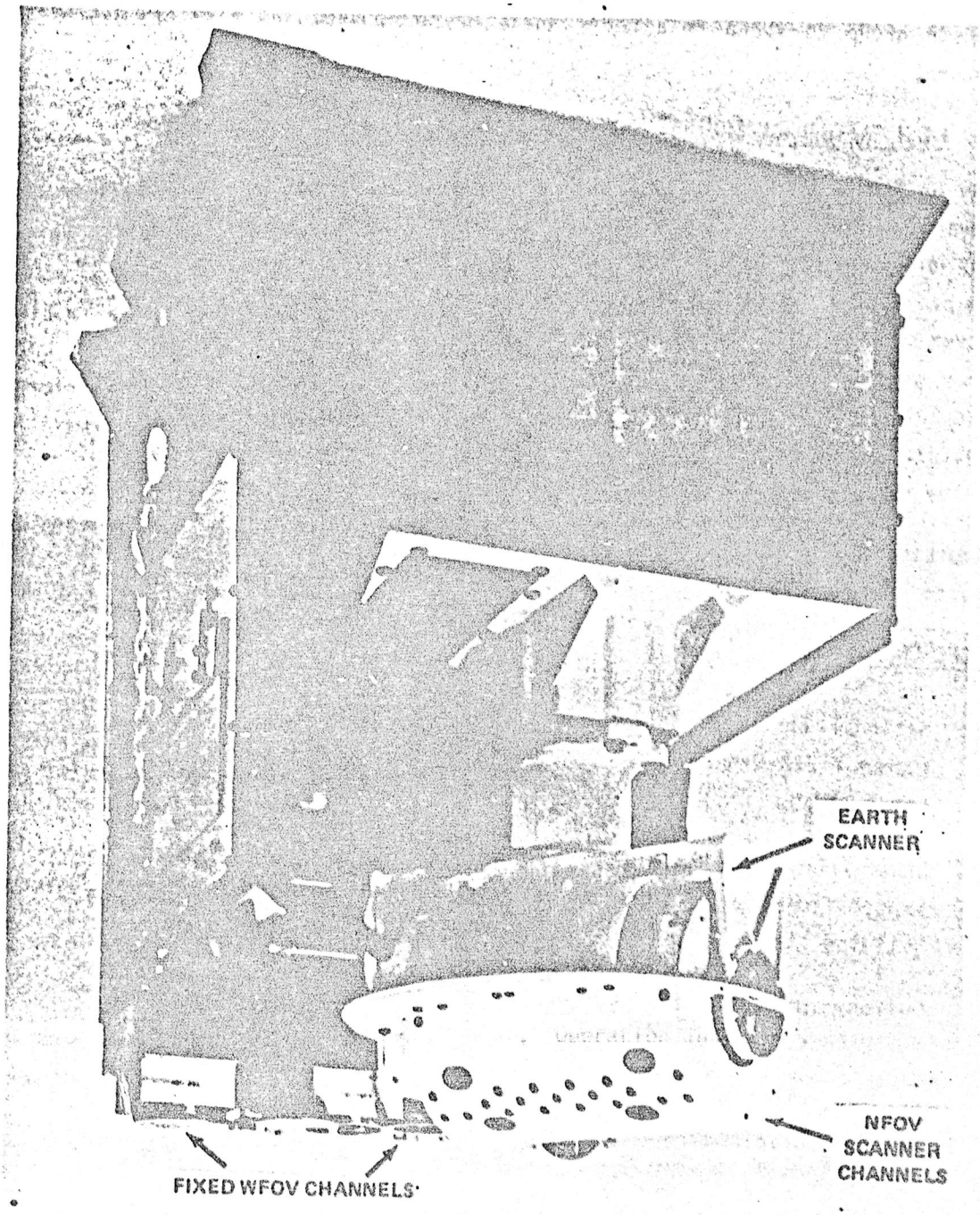

Figure C-4. Assembled Scan Hardware

sensor group to sweep to a nadir angle of 55 degrees and then symmetrically return.

6. SCAN PATTERN DETERMINATION

The pattern of incremental scan motion was determined by the number of scan advance commands received by a recycling module five counter. If routine five was selected, the pattern determinator called for either pattern three or four, depending on whether motion was occurring during the first or second seven major frames of the pattern. If a SCAN OFF was issued during the routine four portion of routine five and the pattern counter was not advanced, upon receipt of a subsequent SCAN ON command, the pattern generator called forth pattern four, not pattern three, with the remaining three/four alternations being reversed.

Additional details regarding the telescope scanning characterisitcs can be found in References 1 and 3 or in the Nimbus 6 or 7 User's Guide.

REFERENCES

1. National Environmental Satellite Service N AA, "Design Study for the Nimbus F ERB Experiment," Final Report, Phase I, Contract 8-50089A, December 7, 1970.

2. Laser Precision Corp, "Pyroelectric Detectors for the Nimbus F ERB Instrument," Engineering Report RK 121-1, in the NOAA files at World Weather Building, 1972.

3. Gulton, "Operation and Maintenance Manual for the ERB Radiometer Subsystem for Nimbus F," Report 13936-970, Contract 2-35297, 1974.

4. Ruff, I., "ERB Scanning Channel FOV Alignment," in the NOAA files at World Weather Building.

APPENDIX D

MATERIALS SELECTION AND TESTING

APPENDIX D

MATERIALS SELECTION AND TESTING

1. FABRICATION MATERIALS[1]

In Phase I of the initial ERB-6 program, all materials to be used in the solar and earth-flux channels were screened, researched, and tested to ensure the long-term stability of the instrumentation in orbit. Many of the tests were performed by the Materials Research and Development Branch (MRDB) of NASA/GSFC. Vacuum characteristics of paints, adhesives, lacquers, sealants, and primers were considered. Two of the major results were that Eppley-Parson's black usually could not be used. The MRDB scientists recommended a curing procedure for the special varnish that allowed its continued use in sealing the thermopiles. A number of oven bakeout, curing, and vacuum bakeout operations were used in the manufacturing process. Thus, all of sensor surfaces were blackened using 3M-401C10 velvet black paint. The required bakeout operations were used in the manufacturing process. The required bakeout procedures were performed in a vacuum of 10^{-6} torr. Although better blacks for cosine response and high absorptivity, such as Parson's black and some gold blacks, were available, they did not meet space-use criteria.

Thermal surfaces of the channel modules and the interfaces to the experiment frame were coated with Emerson and Cummings-type TC-4 grease to ensure good thermal contact under vacuum conditions.

The black coating of the interior channel walls and baffles presented a problem because of the difficulty in applying the paints to the small reflection-reducing grooves. A black-anodizing process using inorganic dyes was investigated and used. Normal black anodizing was not acceptable because of its optical characteristics and vacuum environment considerations.

The coating of the solar-facing surfaces had to be one with a low solar absorbance. Polished aluminum surfaces were tested, but it appeared that highly machined surfaces were satisfactory for the small cross-sectional areas presented by the outer rings of these channels.

2. OPTICAL MATERIALS

The optical materials had to withstand the Nimbus orbit environment for a long period of time (at least 1 year) without suffering changes in their transmission properties. These materials were exposed to solar ultraviolet as well as to particle radiation. The primary optical material used in the channels was fused silica. A program was conducted in the design study phase to determine the best possible fused silica for use in the experiment. After a literature and material availability data search, it appeared that Corning type 7940,* Dynasil 1000,† and Suprasil W‡ fused silicas were the best materials for windows and interference filter substrates. Of these, Suprasil W appeared best in withstanding the particle radiation environment; further, it exhibited the best transmission characteristics in the near infrared since the typical 2.7-μm OH absorption band was not present. Obtaining Suprasil W, of the highest quality, was a problem at that time because the manufacturer had discontinued the process, apparently as a result of a lack of a market. However, it was agreed that they would produce sufficient stock for the ERB experiment.

All the foregoing fused silicas, plus Infrasil,* were tested for damage caused by the anticipated particle and UV radiation levels of the Nimbus orbit. Radiation levels were chosen based on the Nimbus orbit parameters. Particle fluences and energies for both electrons and protons were supplied by the Theoretical Studies Branch of NASA/GSFC. Samples were exposed in vacuum, and it was found that for the projected 1-year Nimbus life period, no significant changes occurred in the transmittance of the fused silicas due to particle radiation. It was also determined that the fused silicas in sufficient thickness would be used to prevent particle radiation induced damage to the Schott colored glasses and to the multilayer materials of the interference filters. Therefore, no transmittance changes were expected in the case of the ERB optical elements.

---

*Corning Glass Corporation
†Registered trade name of Dynasil Corporation of America
‡Manufactured by Englehard-Hereaus-Schott, Hanau, West Germany

The results of UV exposure testing, in vacuum, presented another problem since all the fused silicas showed some changes as a result of exposure to simulated solar radiation. Suprasil W exhibited the least effect, followed by Corning 7940 and then Dynasil 1000 and Infrasil II. It appeared that the original choice of Suprasil W was appropriate. Consideration has been given to "pre-aging" the substrates before use for the final filters, because the decrease in transmittance with time leveled off after about 1200 equivalent UV solar hours.

The Schott glasses showed no degradation due to UV radiation. Two of the pre-prototype interference filters exhibited transmittance depletion because of UV exposure, which appeared to be in excess of that caused by the substrate material, Dynasil 1000. It is not certain what caused the degradation since other filters of similar construction did not show any effect.

3. INTERFERENCE FILTERS

The most desirable transmittance curve for filter radiometric applications is a sharp cut-on, flat top, and sharp cut-off (i.e., ideally a square wave). This is seldom realizable for deposited interference filters. Filters must reject radiation outside the main transmission band to the extent that the total irradiance at the thermopile receiver, because of out-of-band transmitted energy over the entire solar spectrum, is less than one half of 1 percent.

Since the ideal shape cannot be realized, filter factors (reciprocal of the effective transmittance) must be such that for all possible extraterrestrial solar spectral distributions over the pertinent filter bands, they should not differ by more than a fraction of 1 percent. For example, in the λ = 0.250-0.300-μm extraterrestrial band, where considerable measurement differences between various investigators exist, the variation in filter factor for the ERB-6 channel 10S filter must be nearly the same for the two most different solar curves. Since the curve shape rather than the absolute spectral irradiance is the critical consideration here, the two curves that differ most in this manner are the most important.

REFERENCE

1. Hickey, J. R., "A Satellite Experiment to Establish the Principal Extraterrestrial Solar Energetic Fluxes and Their Variance," in Extraterrestrial Solar Spectrums edited by A.J. Drummond, et al., Inst. of Envir. Sci., 1973.

APPENDIX E

TEST AND CALIBRATION PROGRAMS

APPENDIX E

TEST AND CALIBRATION PROGRAMS[1]

The high precision and accuracy requirements of the experiment demanded that a comprehensive test and calibration program be performed on components, finished modules and the overall ERB sensor system.

1. COMPONENT TESTING

The test program began with the receipt of raw materials. Optical materials were tested for transmittance over the pertinent spectral bands, optical quality, and proper size before being used for fabrication of windows, filter substrates, or hemispheres. Thermopiles were tested a number of times during manufacture to ensure that the resistance of the wire and the isolation from the body were correct for each step in the manufacturing process. Glass and fused silica windows were tested for the variation of transmittance with angle of incidence over the range of the FOV of the appropriate channel. The effect of temperature on the short-wave cut-on of the colored glass was measured over the range of 0° to +50° C. These latter tests were performed to obtain correction information for use during both the calibration and the actual experiment data evaluation programs.

Tests on interference filters included normal and off-axis transmittance measurements and changes with temperature. In addition, tests for secondary transmittance were performed in an operational as well as in a spectrophotometric manner. In the former instance, the integral transmittance of the filter, as irradiated by a solar simulator beam, was monitored by a pyrheliometer, selective sharp cut-on glass windows being used to shutter the primary transmission region while allowing at least 90 percent of the energy in the suspected secondary transmission region to reach the filter. The uniformity of transmittance over the free aperture region of the filter area was also monitored using small masks.

Tests on completed thermopiles included the evaluation of (1) vacuum-air ratio of responsivity; (2) linearity over the dynamic range of response; (3) time-constants of the active and reference receivers; (4) temperature dependence of

responsivity over the operational temperature ranges in air and vacuum, and (5) preliminary air responsivity (determined as the last step in test procedure after the thermopile has been mated with the appropriate module body). Here, "air" refers to an atmospheric pressure, and "vacuum" refers to a pressure of 10^{-6} torr or less. Table E-1 indicates the thermopile characteristics in air and a vacuum.

Table E-1
ERB Thermopile Characteristics

Characteristic*	Type	
	N3	K2
Irradiance Responsivity or Sensitivity ($mV/mW\ cm^{-2}$)		
(a) In Air	0.098	0.750
(b) In Vacuum	0.127	1.310
Vacuum/Air Ratio (Unitless)	1.300	1.750
Time Constant		
(a) Air (sec)	1.000	3.000
(b) Vacuum (sec)	1.200	4.000
Resistance (Ω)	820.000	5000.000
Inductance (mH)	3.500	30.000
Capacitance†		
(a) Across contacts (μF)	1.900	0.200
(b) To body (pF)	330.000	<10.000

*All characteristics vary somewhat from unit to unit; values here are averages.

†Note change of units between (a) and (b).

A set of Angstrom electrical compensation pyrheliometers calibrated against the international reference, in Davos, Switzerland, was used as standards for the total short-wave and broad-bandpass channels. Normal incidence

(thermopile-type) pyrheliometers that had been calibrated against the Eppley standards and that were fitted with matching filters were used for calibrating the interference filters. Obviously, the two channels having the shortest wavelength bands could not be intercompared in natural sunlight at the Earth's surface and therefore were calibrated with simulated solar radiation.

With all solar channel calibrations in natural sunlight, corrections were made for the effects of atmospheric turbidity (16) and FOV differences (17) to account for the different amounts of the circumsolar sky radiation accepted by the reference and test detectors. Corrections for the variation of filter factor with respect to the various terrestrial and simulated solar curves were made.

The RSM transfer calibration method was based on (1) no short-wave source being considered sufficiently stable to serve as a primary transfer device "as pertains to the ERB performance specifications and required calibration accuracies," (2) a thermopile element being regarded as the most reliable and stable operational radiation detector available for use in transfer calibrations of the type required for the ERB radiometer, and (3) the geometry of transfer calibrations being easily maintained when both instruments involved in the transfer were of similar construction.

1.1 EARTH-FLUX CHANNELS

Calibrations of channels 11E and 12E were of two types: long-wave and short-wave. The long-wave (IR) calibrations were performed using a special blackbody source. The short-wave calibrations of the earth-flux channels of the RSM instruments were performed in the integrating hemisphere for diffuse radiation and at the observatory by use of direct solar beam occulting. For channels 11E and 12E, special Suprasil W partial hemispheres were used during short-wave calibrations.

Channels 13E and 14E were calibrated in the same manner as the foregoing short-wave calibrations, with the exception that RG695 matching glass was used on both the pyrheliometer and pyranometer standards of calibration of 14E.

1.2 STIMULI EQUIPMENT

There are two basic types of stimuli equipment for the earth-flux channels. The first is the Total Earth-flux Channel Blackbody (TECB). It was a double-cavity blackbody unit designed for calibrating both channels 11E and 12E after they were mounted to the ERB package. It operated over the range 180 to 390 K with an apparent emissivity under test conditions, in vacuum of 0.995 or greater. Its design was based on the use of the surfaces of the channel being calibrated as an integral part of the blackbody. The FOV's of both channels were filled during this calibration. Temperatures were measured to 0.1°C and controlled to that accuracy in the ERB-6.

The Short-wave Earth-flux Channel Comparator (SECC) was used for intercomparing channels 13E and 14E of a flight instrument with the matching channels of the RSM. It consisted of a four-aperture light box assembly with a single quartz halogen lamp source having a tungsten filament. The primary light beam was directed to each of the four channels by a rotating mirror assembly.

The primary piece of stimuli equipment for intercomparing the RSM and flight instrument solar channels was the solar simulator that had a Xenon arc as a source. Solar spectral match was provided by filters. A spectral matching filter used for channels 1S through 8S was removed for the intercomparisons of channels 9S and 10S.

2. THERMAL ANALYSIS

Based on an early estimate of thermal transients during the on-sun-measuring periods, the necessity of obtaining the best possible balance between active and reference junction thermal time constants was established. Once balanced as a unit, the thermopile transient offset signals were those caused by selective heating or cooling within its view (not the channel FOV). To prevent such radiational thermal offset effects, the rear of the thermopile was encased, without contact, in a copper-base, gold-plated shield device to ensure that the reference receiver did not produce a signal because of a transient radiational surrounding.

The situation for the active receiver was somewhat more difficult to control because no such shielding could be used without jeopardizing the mission.

Thus, both the conductive and radiation transients were reduced by careful analysis and testing. The channels in which the greatest possibility of transient offset was possible were 9S and 10S due to radiational effects and channels 6S, 7S, and 8S because of conductive transients.

REFERENCE

1. Hickey, J. R., "A Satellite Experiment to Establish the Principal Extraterrestrial Solar Energetic Fluxes and Their Variance," in Extraterrestrial Solar Spectrums, edited by A. J. Drummond, et al., Inst. of Envir. Sci., 1973.

END

DATE

FILMED

MAY 3 1983